Multi-temporal tectonic evolution of Capo Granitola and Sciacca foreland transcurrent faults (Sicily channel)

L. Ferranti[1a, 2b, 3c, *]

lferrant@unina.it

F. Pepe[4d]

G. Barreca[2b, 5e]

M. Meccariello[1a, 2b]

C. Monaco[2b, 5e]

[1a]Dipartimento di Scienze della Terra, dell'Ambiente e delle Risorse, Università di Napoli "Federico II", Napoli, Italy

[2b]CRUST - Centro inteRUniversitario per l'analisi SismoTettonica tridimensionale con applicazioni territoriali, Italy

[3c]INGV-Sezione Roma 1, Italy

[4d]Dipartimento di Scienze della Terra e del Mare (DISTEM), Università di Palermo, Palermo, Italy

[5e]Dipartimento di Scienze Biologiche, Geologiche e Ambientali, Università of Catania, Catania, Italy

*Corresponding author.

Abstract

Joint analysis of high-penetration multi-channel and high-resolution single-channel seismic reflection profiles, calibrated by deep well boreholes, allowed a detailed reconstruction of the Late Miocene to Recent tectonic history of the Capo Granitola and Sciacca fault systems offshore southwestern Sicily. These two fault arrays are part of a regional system of transcurrent faults that dissect the foreland block in front of the Neogene Sicilian fold and thrust belt. The Capo Granitola and Sciacca faults are thought to reactivate inherited Mesozoic to Miocene normal faults developed on the northern continental margin of Africa. During Latest Miocene-Pliocene, the two ~NNE-SSW striking faults were active in left transpression, which inverted Late Miocene extensional half-grabens and created push-up ridges along both systems. Tectonic activity decreased during the Pleistocene, but transpressional folds deform Middle-Late Pleistocene sediments as well, suggesting that the two fault systems are active. The ~40–50 km long longitudinal amplitude profile of 1st order folds (Capo Granitola and Sciacca anticlines) shows ~105-20–30 km bell-shaped undulations that represents 2nd order folds. The length of these undulations together with the map pattern of faults allowed to divide the CGFS and SFS into two segments, northern and southern, respectively. Total uplift of the Sciacca Anticline is twice than the uplift of the Capo Granitola Anticline. Incremental fold growth rates decreased during time from 0.22 mm/yr (Capo Granitola Anticline) and 0.44 mm/yr (Sciacca Anticline) in the Pliocene, to 0.07 and 0.22 mm/yr, respectively, during the last ~1.8 Ma.

Keywords: Multiscale analysis; Basin inversion; Strike-slip faults; Fold growth rates; Pelagian foreland; SW Sicily offshore

1.1 Introduction

The Sicily Channel between Sicily and North Africa crosses the boundary between the Sicilian-Maghrebian orogen and the Pelagian foreland of the African continental margin (Fig. 1). Foreland domains are commonly considered to be little deformed or at most affected by long-wavelength tectonic structures (e.g. DeCelles and Giles, 1996). In contrast, narrow structural belts where tectonics has been intense, crosscut the Pelagian foreland (Fig. 1). These structural belts include NNE-SSW striking strike-slip faults offshore and on-land southern Sicily and NW-SE striking normal faults in the axial rift of the Sicily Channel (Fig. 1; Argnani et al., 1986; Antonelli et al., 1988; Civile et al., 2014; Cavallaro et al., 2017; Ghisetti et al., 2009).

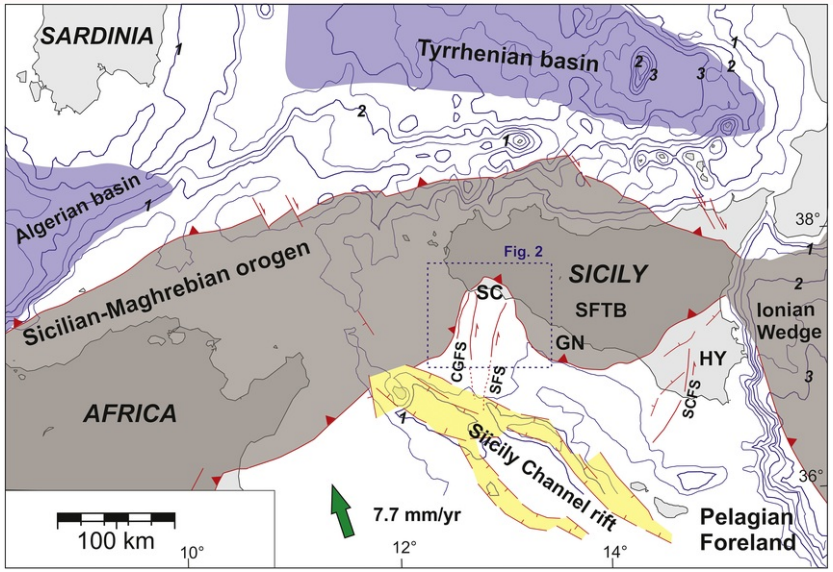

Fig. 1

alt-text: Fig. 1

Offshore the southwest coast of Sicily, post-Late Miocene deformation related to Africa and Europe plate convergence has been distributed between the frontal thrust belt and two regional transcurrent faults in the foreland domain, namely the Capo Granitola and Sciacca fault systems (CGFS and SFS, respectively; Figs. 1, 2). The CGFS and SFS are viewed as inherited crustal discontinuities that evolved along the North African margin during Mesozoic and Cenozoic (Argnani et al., 1986; Ghisetti et al., 2009; Di Stefano et al., 2015; Civile et al., 2018).

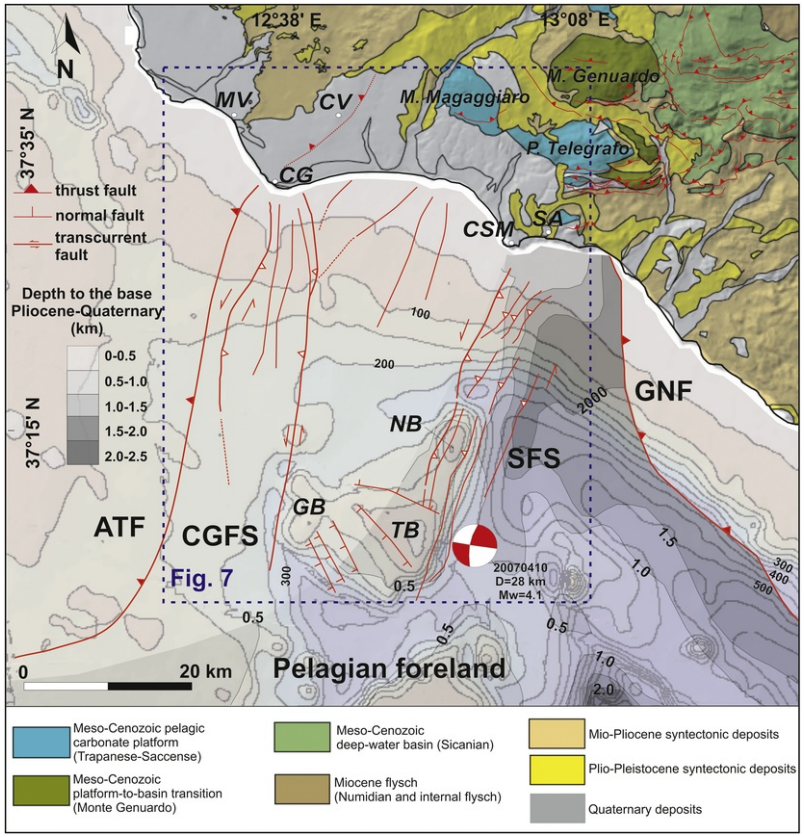

Fig. 2

alt-text: Fig. 2

Previous reconstructions of the tectono-stratigraphic evolution of the southwest Sicily offshore chiefly relied on high-penetration multichannel seismic (MCS) profiles provided by industry exploration during the ‘80s of the last century (Argnani et al., 1986; Argnani, 1987; Antonelli et al., 1988; Fedorik et al., 2017). According to Fedorik et al. (2017), the CGFS is presently inactive whereas the SFS is active only in its southern part where the structure has a bathymetric expression. Civile et al. (2018) presented newly acquired MCS profiles that allowed them to map at a better resolution the structural asset of the two fault systems. They integrated MCS data set with high-resolution Chirp profiles that provided evidence of active deformation along the CGFS and the northern part of the SFS as well (Fig. 2). However, this evidence is too sparse to support a comprehensive analysis of the role of the CGFS and SFS in the current deformation field and to tie the long- and short-term tectonics history of the two faults.

Barreca et al. (2014), based on geodetic and archeoseismological data, pointed out that thrusting and folding still occurs along the on-land continuation of the ATF north of Capo Granitola (Fig. 2). Thus, the current ~NNW-SSE oriented plate convergence appears to be accommodated both by reverse motion along the front of the SFTB and by left-transpression along the foreland transcurrent faults.

In this paper, we present a joint analysis of high-resolution single-channel (SCS) profiles and high-penetration multi-channel (MCS) seismic profiles available from the Vi.De.Pi. Project (http://unmig.sviluppoeconomico.gov.it) and from the ENI databases, calibrated with deep well boreholes. Our study is based on a multiscale analysis of the geometry and evolution of the fold systems related to the CGFS and SFS and provides evidence of recent and active tectonics in the area between Capo Granitola and Sciacca (Fig. 3). Following the approach used in similar context offshore southern Italy (e. g. Ferranti et al., 2014), w~~W~~e complement the geometric reconstruction of the main structures with a quantitative analysis of vertical displacements of structures related to these two fault systems to single out the temporal variations in deformation and evolution of fault segmentation.

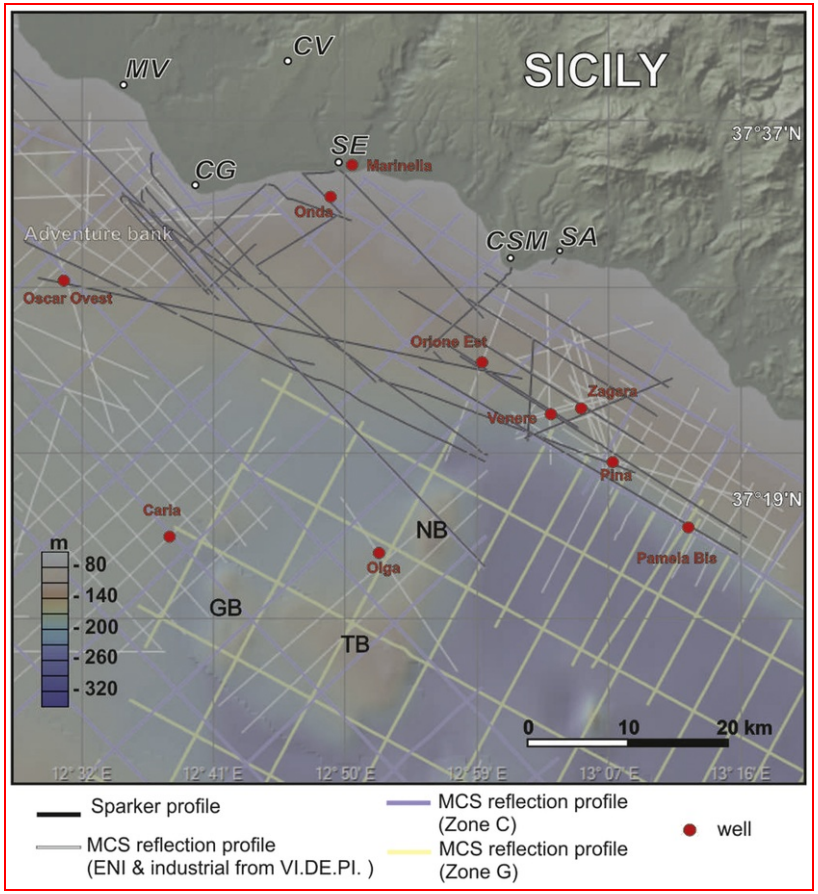

Fig. 3

alt-text: Fig. 3

~~2.~~2 Tectonic background

The tectonic evolution of this sector of the Central Mediterranean is related to ~NNW-SSE convergence between Africa and Europe, which led to the closure of the Tethyan ocean and collision between the European and African continental margins. The Sicilian fold and thrust belt (SFTB) is mainly composed of imbricates of Mesozoic-Cenozoic carbonate platform and basin rocks of the ancient African margin, and of their Neogene synorogenic cover (Catalano et al., 2002, 2013). Age and facies correlative pre-orogenic rocks are found in the Pelagian foreland domain.

Seismic reflection profiles, deep well boreholes and field observations document that the SFTB in central-western Sicily is composed of two superposed structural levels (Catalano et al., 2013). The upper level is made of an ~2–3 km thick stack of detached, thin thrust sheets involving deep-water rocks (Imerese and Sicanian units). During the Miocene, this stack was thrust over thick platform carbonates of the Trapanese and Saccense units, that form the lower level. Starting from Late Messinian (Latest Miocene), the lower level was itself involved in shortening accommodated by deep-seated thrust ramps that enucleated large-wavelength anticlines and passively refolded the previous structural fabrics (Oldow et al., 1990; Avellone et al., 2010). Overall, the thickness of the orogenic wedge increases toward the north and reaches 25 km or thicker on the northern shore of the island (Catalano et al., 2013).

The foremost advanced part of the thrust belt is found in central-southern Sicily and in its offshore, where it forms the ~2–3 km thick Gela Nappe (Fig. 1). The latter is composed by imbricated Miocene Numidian flysch and clay carbonate Mesozoic-Cenozoic Sicilidi rock units and Tortonian-to-Pliocene deposits units thrust above Tortonian to Lower Pleistocene deposits that stratigraphically overlie the Pelagian Mesozoic to Cenozoic carbonates (Argnani, 1993; Lickorish et al., 1999; Ghisetti et al., 2009).

Just ahead of the thrust front, the northern part of the Pelagian foreland is cut by two ~NNE-SSW trending regional strike-slip fault zones that bound to the east and west the arcuate front of the Gela Nappe (Fig. 1). The aggregated CGFS and SFS, which cut across the largely submerged Saccense part of the Pelagian foreland, represents the western fault system. The Scicli Fault forms the eastern fault system and runs across the emergent Hyblean foreland plateau. The Saccense and Hyblean foreland sectors are made of stiff Mesozoic-Cenozoic carbonate platform rocks. Conversely, Mesozoic-Cenozoic basinal clays are buried beneath the Gela Nappe and the frontal thrust belt. According to Lickorish et al. (1999) and Ghisetti et al. (2009), the two carbonate blocks formed rigid salient that limited the propagation of the thrust front. Instead, a larger southward advancement of the Gela Nappe occurred above the fault-bounded basinal depression between the two foreland indenters of the lower plate (Lickorish et al., 1999). In this scenario, the transcurrent fault zones and normal faults that accommodated northward flexure of the Hyblean and Saccense blocks likely contributed to convey the migration of the Gela Nappe to the south.

Although the nature of the foreland shear zones is poorly established, they are thought to be inherited Mesozoic normal faults that cut the basement and formed along the rifted passive margin of the Permo-Triassic Ionian Tethys (Catalano, 1982; Di Stefano et al., 2015). These faults continued moving as normal or transtensional until Late Miocene during coeval advancement of the SFTB and underwent transpressional reactivation since then (Argnani et al., 1986; Antonelli et al., 1988; Argnani, 1993; Ghisetti et al., 2009; Civile et al., 2018). During the most recent (post early Pliocene) deformations, the ~N-S reactivated basement faults deformed the base of the Gela Nappe itself (Ghisetti et al., 2009). Reactivation of older normal faults that strike at high-angle to the thrust front is viewed as due to flexural inflection of the foreland plate beneath the advancing thrust belt (Cogan et al., 1989; Grasso et al., 1995), which varied laterally within adjacent blocks with strong inherited changes in crustal thickness (Reuther et al., 1993).

The western or Saccense salient is bound to the west by the Adventure Thrust Front (ATF), which limits the southeast-verging SFTB, and to the east by the front of the south-verging Gela Nappe (Fig. 2). The Adventure Thrust Front probably continues onshore between Capo Granitola and Castelvetrano, where a ~NNE-SSW trending thrust-related anticline is developed in Pleistocene deposits and is associated with archeoseismic evidence of deformation (Barreca et al., 2014). The apical sector of the salient is formed by an ~ESE-WNW array of thrust faults in the Monte Magaggiaro-Pizzo Telegrafo area (Fig. 2). Within the concave side of the arcuate thrust front, the foreland domain is sliced by the CGFS and SFS left-transpressional fault systems (Fig. 2; Argnani et al., 1986; Antonelli et al., 1988; Argnani, 1993; Grasso, 2001; Civile et al., 2018). The salient forms a bathymetric and structural culmination compared to the regional depression east of the SFS, where a >2 km thick Pliocene-Quaternary succession is overthrust by the Gela Nappe (Fig. 2). Within the culmination, two narrow belts of structural highs reflecting positive flower structures are found along the CGFS and the SFS.

The CGFS in the west is composed of two sub-parallel, ˜N-S trending faults. The SFS in the east is structurally more complex and consists of a sub-vertical NNE-SSW trending master fault and associated splays (Fedorik et al., 2017). To the south, the two transcurrent faults dies out against or interact with NW-trending Late Miocene and younger normal faults that bound submarine banks (Fig. 2). These normal faults are viewed as part of the Sicily Channel axial rift system (Fig. 1).

The northward continuation of the two foreland faults beneath the thrust belt on-land Sicily is not fully understood. The submerged expression of the transcurrent faults terminate at about the coastline (Fig. 2), and north of there they likely dip beneath the thrust belt together with the foreland. According to Di Stefano et al. (2015), a currently active N-S crustal discontinuity runs in western Sicily from the northern to the southern shore roughly orthogonal to the thrust belt. In their view, this right-lateral shear zone reactivates a paleogeographic boundary that formed during Permo-Triassic and separated a thick continental crust to the west, where carbonate platforms developed, from a thinned continental crust covered by deep-water carbonate deposits to the east. Although this crustal discontinuity could control the deep crust and upper mantle seismicity (e.g., Calò and Parisi, 2014), its upper crustal expression is not revealed by geological and geophysical data because of the structural superposition of the thrust belt above (Fig. 1).

Sparse seismicity is recorded along the transcurrent belt (Calò and Parisi, 2014). The most energetic events are broadly located in the southern part of the SFS and have focal mechanisms consistent with left-lateral strike-slip motion on the fault array (Fig. 2; Soumaya et al., 2015).

~~3.~~3 Materials and methods

We based our study on the integration of geophysical datasets including: a) an irregular, but locally dense, grid of newly acquired high-resolution, single-channel, seismic reflection profiles and b) high-penetration, multichannel seismic reflection profiles made available by ENI Exploration & Production and by the Vi.DE.PI database (http://unmig.sviluppoeconomico.gov.it/videpi/sismica/sismica.asp).

The acoustic source for seismic prospecting was a 1 kJ Geo-Source Sparker, with a multi-tip Sparker array and a single-channel streamer having an active section of 2.8 m, containing eight high-resolution hydrophones. The shooting interval was 1.5 s with 1 s records length and 0.1 ms sampling interval. A DGPS system controlled the navigation. Data were acquired in the NW-SE and NE-SW directions (black lines in Fig. 3), which are sub-parallel to regional dip and strike of the tectonic features, respectively.

The adopted processing sequence included the application of the following mathematical operators: spherical divergence correction, de-ghosting, migration, band-pass (200–2000 Hz) filter, swell filter, trace mixing, time variant gain and mute of the water column. Signal penetration was found to exceed 250 ms two-way time (t.w.t.). The vertical resolution is ~0.3 m near the seafloor.

MCS reflection profiles from Vi.DE.PI database (white, violet and yellow lines in Fig. 3) and additional MCS profiles from ENI E&P database (green line in Fig. 3) were acquired for oil exploration in the Italian Commercial Zone C and G. The MCS sections were converted from raster to SEG-Y format using the GeoSuite AllWorks software. The geodetic reference system is the WGS84 with a UTM 33 N projection.

Seismo- and sequence-stratigraphic based analysis facilitated the reconstruction of the depositional architecture of seismic-stratigraphic units. Following the analysis of acoustic facies, the thickness of sediments was derived from time to depth conversion using velocities of 1500 m/s for the water column and seismic velocity values associated with the Upper Miocene-Quaternary sedimentary successions recognised in boreholes (Figs. 4, 5). Seismic profiles were calibrated using well log data, seismic interval velocities and correlation with on-land outcrops.

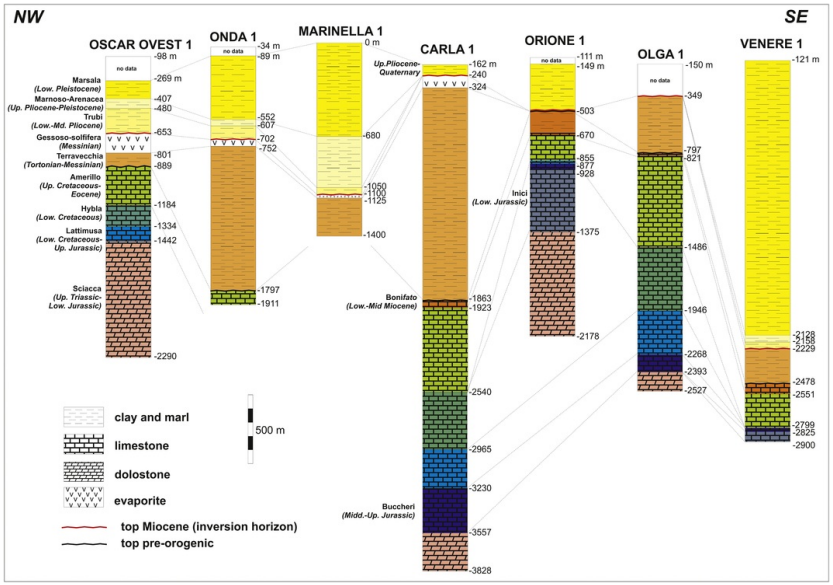

Fig. 4

alt-text: Fig. 4

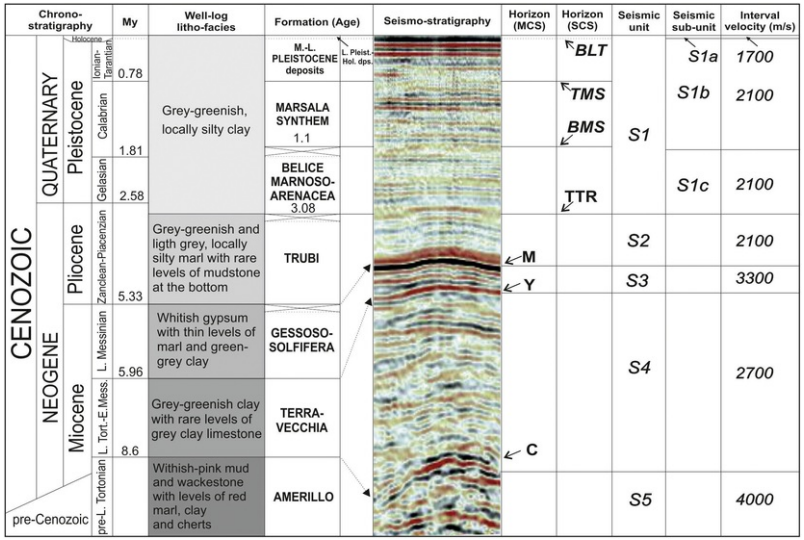

Fig. 5

alt-text: Fig. 5

The orientation of axial surfaces was used to distinguish between drape and growth sequences deposited along the flanks of contractional folds. Axial surfaces dip toward the structural crest in contractional folds, reflecting a state of compression, whereas they are often vertical or dip away from the structural crest in drape sequences reflecting a state of tension and, in some cases, compaction (Laubach et al., 2000).

~~4.~~4 Seismo-stratigraphic and structural interpretation

~~4.1.~~4.1 Seismic stratigraphy

The seismic and sequence-stratigraphic analysis has allowed identifying five seismic stratigraphic units based on their bounding discontinuities, strata architecture and seismic characters (e.g., amplitude, lateral continuity and frequency of internal reflectors). The seismic stratigraphic units were labelled from younger to older as S1 to S5 (Fig. 5).

~~4.1.1.~~4.1.1 *Unit S1*

Unit S1 has layered and parallel, generally sub-horizontal configuration, medium to high-frequency with low-to-medium amplitude reflections (Fig. 5). Calibration of Unit S1 with the stratigraphic succession sampled in the well-logs indicates a correlation with the Pleistocene successions (Figs. 4, 5). We have subdivided unit S1 recognised on SCS profiles into three subunits named S1a, b and c based on their internal geometry and unconformities recognised at the bottom and the top.

Sub-unit S1a exhibits slightly seaward dipping, low- to medium-amplitude and laterally continuous reflections with parallel geometry (Figs. 6a, b). The basal surface of the last transgression (BLT) defines the bottom of S1a. The surface BLT corresponds on the shelf to a regional sub-horizontal erosional surface whereas on the slope it becomes a paraconformity with underlying reflectors. The proximal part of BLT is interpreted as the subaerial erosional surface carved during the LGM at ~18–23 ka when the sea level was ~120–130 m below the present shoreline (Lambeck et al., 2011). Consequently, sub-unit S1a is associated with the Upper Pleistocene-Holocene deposits formed during the transgressive and high-stand stages of the last sea level rise. On the shelf, the thickness of sub-unit S1a averages 15–20 ms (~12–15 m). It reaches the maximum value of ~40 m offshore the fluvial courses, because of an increment of sediment supply.

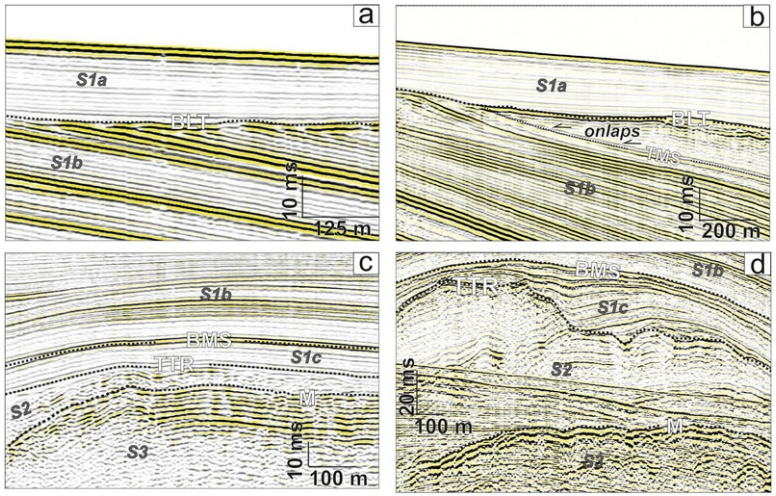

Fig. 6

alt-text: Fig. 6

Sub-unit S1b is represented by a succession of well-stratified, seaward-dipping, high-frequency, medium- to high-amplitude reflections with good lateral continuity (Figs. 6a, b). It exhibits a parallel (the distal portion) to oblique-tangential (the proximal portion) reflectors. The average thickness of sub-unit S1b is ~40 ms (42 m) above structural highs. Calibration of S1b with stratigraphic well-logs indicates that S1b corresponds to the Lower Pleistocene silty clays portions of the Marsala Synthem (Figs. 4, 5). On-land, the Marsala Synthem is dated to the Emilian p.p.-Sicilian p.p. stages (1.1–0.9 Ma) and is represented by cemented carbonate progradational wedges.

In the continental shelf, a discontinuous seismic feature, up to 10 ms thick, ~~characterised~~characterized by chaotic reflections and limited downwards by an erosional or para-conformable surface with underlying reflectors is recognised in the

uppermost part of sub-unit S1b (Fig. 6b). It is interpreted as formed by an amalgamated alternation of regressive and transgressive sequences whose deposition was controlled by the interplay of Middle-Late Pleistocene sea-level changes and low-rate tectonic uplift (e.g. Di Maggio et al., 2017). The contact with underlying tangential and cuneiform reflectors represents the polycyclic erosional surface (Top of Marsala Synthem, TMS, Figs. 5, 6b), which started to form at the onset of the Middle Pleistocene (0.78 Ma). The two seismic packages are continuous and indistinguishable at depths ~~greater than~~ ≥120 m.

A succession of stratified, high-frequency, medium-amplitude and almost continuous reflectors characterise sub-unit S1c (Fig~~s~~. 6c, d). A medium- to high-amplitude with good lateral continuity reflector defines the top of S1c (horizon BMS in Figs. 6c and d). Above reflector BMS, the overlying S1b reflectors show a para-conformable to unconformable contact with S1c reflectors (Figs. 5, 6c, ~~6~~d). On structural highs, sub-unit S1c shows onlap reflectors abutting on top of unit S2. The sub-unit S1c is up to 30 ms (~40 m) thick on structural highs. Based on its stratigraphic position and well-log calibration, we correlate sub-unit S1c with the marly-arenaceous deposits of the Piacenzian p.p.-Gelasian (Late Pliocene-Early Pleistocene) Belice Marnoso-Arenacea Formation (Figs. 4, 5).

In the distal sectors, the aggregated thickness of S1 recognised on MCS profiles reaches 820 ms (840 m, Tab~~.~~le 1). The greater thickness of S1 inferred in MCS profiles and calibrated by well-logs is consistent with the maximum 600~~-~~–700 m aggregated thickness of Pliocene-Pleistocene deposits documented on-land (Basilone, 2012). On the contrary, east of the SFS and the GNF, the thickness of S1 reaches ~~more than~~ ≥2000 m (Fig. 2).

Table 1 Thickness of seismic units in MCS and SCS profiles and in offshore well boreholes. The table shows for comparison the thickness of age-equivalent formations in western Sicily (Basilone, 2012).

alt-text: Table 1

Unit	Unit/Sub-Unit	Formation	Max thickness (structural highs-SCS)		Max thickness (basins-MCS)		Av. thickness western Sicily (m)	Well-log thickness (m)					
			TWT (ms)	Thickness (m)	TWT (ms)	Thickness (m)		Oscar W	Onda	Marinella	Carla	Orione	Venere
S1	S1a	Last Transgression	15~~-~~–20	12~~-~~–17	820	840	x	309	518	680	79	425	2009
	S1b	Marsala Synthem+Mid-Up Pleistocene deposits	35~~-~~–45	36~~-~~–48			50~~-~~–100						
	S1c	Marnoso-Arenacea Belice	30	32			600~~-~~–700	73	150	370		x	
S2	S2	Trubi	80	84	110	115	150	173		50	x	x	101
S3	S3	Gessoso-Solfifera	x	x	100	165	200~~-~~–1000	148	50	25	84	x	x
	S4	Terravecchia	x	x	1300	1800	300~~-~~–1200	88	573	1400+	1531	x	249

On-land, a time-gap between ~1.8 Ma (the top of the Marnoso-Arenacea) and ~1.1 (the bottom of the Marsala Synthem) is recognised between the Marsala Synthem and underlying Belice Marnoso-Arenacea Formation (Basilone, 2012).

~~4.1.2.~~4.1.2 *Unit S2*

A succession of low- to medium-amplitude reflections with medium lateral continuity characterise Unit S2 (Figs. 6c and d). A medium-amplitude, laterally continuous reflector defines its top (TTR in Fig. 5). TTR is an erosional surface on structural highs (Fig. 6c, d).

Based on the stratigraphic position, seismic signature and calibration with well-logs, we correlate Unit S2 with the Zanclean-Piacenzian p.p. (Lower-Middle Pliocene) pelagic limestones and marls deposits known in Sicily as Trubi Formation (Figs., 4, 5). The thickness of S2 is ~70~~–~~–80 ms (~74~~–~~–84 m) on structural highs, an estimate consistent with drilled logs (Tab~~.~~le 1). Differently, in distal sectors, S2 is up to 110 ms thick (~115 m). On-land, TTR marks a stratigraphic time lag between ~3.1~~-~~–2.6 Ma (Basilone, 2012).

~~4.1.3.~~4.1.3 *Unit S3*

Unit S3 exhibits continuous, medium- to high-frequency and medium-amplitude reflectors with layered parallel to locally divergent geometry (Fig. 5). It is bounded at the top by the well-defined, high-amplitude reflector M, a horizon of regional importance associated with the top of evaporites deposited during the late Messinian salinity crisis and/or with an erosional unconformity formed during the late Messinian sea level fall (Finetti and Morelli, 1973; Malinverno et al., 1981). Unit S3 is correlated with Upper Messinian evaporites and associated clastic deposits of the Gessoso-Solfifera formation (Figs. 4, 5). The maximum thickness of unit S3 is 150 m (Tab~~.~~le 1).

~~4.1.4.~~4.1.4 *Unit S4*

Unit S4 is typified by low- to medium-frequency and low to medium-amplitude reflectors with low- to moderate-lateral continuity and locally divergent geometry (Fig. 5). A medium-amplitude, laterally continuous reflector (horizon Y, Fig. 5) define its top. A moderately continuous, high-amplitude reflector (horizon C, Fig. 5) limits unit S4 downwards. It corresponds to a lithologic change or an erosional surface (Ghisetti et al., 2009; Civile et al., 2014; Cavallaro et al., 2017) that marks the contact between the top of pre-orogenic carbonates and the base of Middle-Upper Miocene synorogenic silty-clay deposits (Fig. 4). We attribute unit S4 to the Tortonian-Lower Messinian clay, sandstone and occasionally clay-limestone of the Terravecchia Formation (Figs. 4, 5). Unit S4 has a highly variable thickness reaching ~~more than~~ ≥1.5 km in the depocenters of the basins (Tab~~.~~le 1 and Fig. 4).

~~4.1.5.~~4.1.5 *Unit S5*

The seismic succession that underlies reflector C is labelled as S5 (Fig. 5). Its age varies from Cretaceous to Early-Middle Miocene (Fig. 4). For the aim of this paper, we do not provide further details on unit S5.

~~4.2.~~4.2 Capo Granitola Fault system

Structural interpretation of MCS profiles documents that the CGFS extends from Capo Granitola to the western side of Graham Bank for a total length of ~40~~–50~~ km (Fig. 7; Tab~~.~~le 2). The CGFS has an N-S trend ~~in the north~~off Capo Granitola and gently swings to an NNE-SSW trend and widens from ~~~5~~10 to ~1~~0~~5 km in the south. The fault system becomes less evident southwards and vanishes south of the Graham Bank.

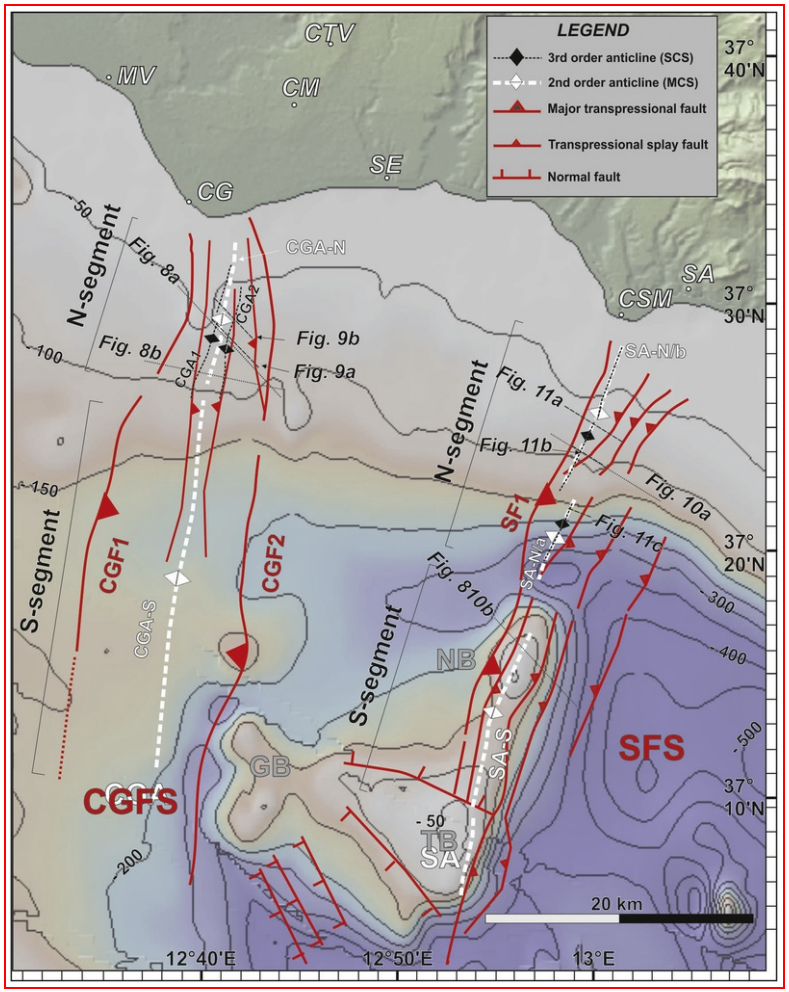

Fig. 7

alt-text: Fig. 7

Table (I would like to slightly modify the Table but I was not able to do it in the proofcentral system. I upload the revised Table 2)2 Geometric parameters and structural ~~hyerarchy~~ hierarchy of the Capo Granitola and Sciacca Fault Systems.

alt-text: Table 2

Fault System	Major Fault Array	Cumulative lngth (km)	Fault CGF1	Length (km)	Fault CGF2 & SF1	Length (km)	Max reverse throw (m) on M	1st Order Fold	Length (km)	Post-linkage Amplitude (m) on horizon M	2nd Order Fold	Length (km)	Pre-linkage Amplitude (m) on horizon M	Estimated linkage timing (Ma)	3rd Order Fold	Length (km)	Fold Amplitude (m) on horizon BMS/TMS
Capo Granitola Fault System	CGF1 & CGF2	50	Northern segment	12	Northern segment	15	240	Capo Granitola Anticline	42	730	CGA-North	10	170	3.7~~-~~–4.5	CGA1	8	80
			Southern segment	30	Southern segment	32	270								CGA2		30
											CGA-South	22	190		-	-	-
-Sciacca Fault System	SF1	48	-	-	Northern segment	20	-	Sciacca Anticline	50	1040	SA-North	18	850	2.2~~-~~–3.4	SA-N/b	9	170
			-	-											SA-N/a	9	130
			-	-	Southern segment	27	-				SA-South	>20	980		-	-	-

The CGFS is ~~characterised~~characterized by a structural high floored by a broad box-fold (Capo Granitola Anticline, CGA, Fig. 7) that does not have a bathymetric expression (Fig~~s~~. 8a, b). ~~T~~Locally, three ancillary folds are found on top of the anticline (CGA1, CGA2, CGA3, Fig. 8a). Two high-angle faults labelled CGF1 (the western) and CGF2 (the eastern) bound the CGA (Fig. 7) and display a reverse component of motion. Minor faults are traced between CGF1 and CGF2 in the northern part of the CGFS (Figs. 7, 8a, 8b).

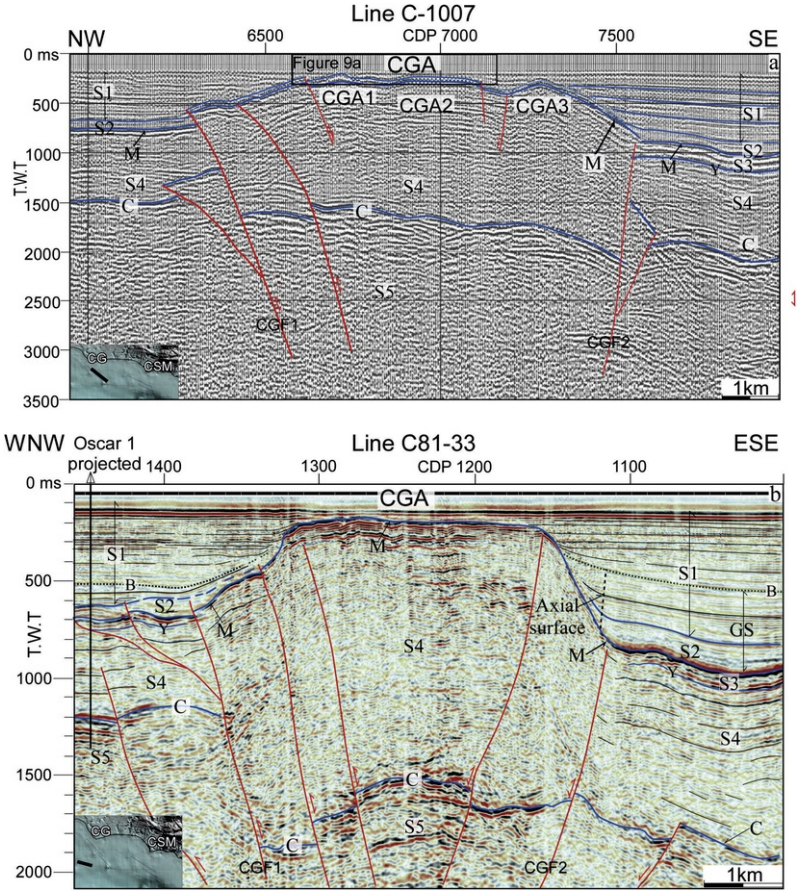

Fig. 8

alt-text: Fig. 8

The complex history of the structural high is deciphered through analysis of thickness variations, the geometry of deposits and the dip of fold axial surfaces. Tortonian-Lower Messinian deposits display a marked change in thickness moving from the core to the flanks of the CGA. The sequence thickens to a maximum value of ~1300 ms (~1800 m) beneath the CGA while maximum thickness reduces to ~450 ms (~600 m) and ~1000 ms (~1350 m) in the western and eastern footwall blocks, respectively (Figs. 8a, 8b). The abrupt thickness change of up to ~1 s in correspondence of fault CGF1 suggests that, during part of Tortonian-Early Messinian, the current high was a basin bounded by faults that had an extensional component.

On the top, M appears to be an erosional surface, but it grades in the basin to the top of evaporitic basin deposits (Unit S3) as suggested by the Oscar W well on the western flank (Fig. 8b). In this scenario, a bathymetric high, possibly emerging above the sea-level could have formed in Latest Miocene before or during the Late Messinian salinity crisis (~6–5.3 Ma). This observation suggests the onset of basin inversion.

Growth geometries of Pliocene-Early Pleistocene deposits (unit S2 and sub-unit S1c) on the flanks of the Capo Granitola Anticline (dotted line marked with B, Fig. 8b) and the axial surfaces dipping toward the crest of the fold document that inversion occurred at high-rate during this time interval. Because of the low-resolution of the MCS profiles, reflectors in the upper part of S1 appears to onlap the anticline on each side (Figs. 8a, b).

Clues on the age of deformation and geometries of the secondary anticlines CGA1 and CGA2 derive from the SCS profiles that show at high-resolution the minor folds recognised in MCS profiles on top of the larger-scale anticline (Fig. 8a). These folds have an NNE-SSW trend, a wavelength of ~1 km and are mapped for a ~10 km length (Fig. 7; Table 2).

Pre-S1 reflectors in the core of CGA2 are folded with a box-like geometry (Figs. 9a, b), in a manner consistent with the large-scale structure (Figs. 8a, 8b). Upper Messinian deposits (unit S3), which cores the folds, are overlain disconformably or paraconformably by Lower-Middle Pliocene (unit S2) pelagic limestones and marls deposits. They are ~~recognized~~recognised along the flanks and on tops of both folds, where they are strongly folded, eroded, and occasionally thickened by thrust faults. Upper Pliocene-Lower Pleistocene deposits (unit S1c) display growing relations on the flanks of both CGA1 and CGA2, whereas they unconformably overlie Lower-Middle Pliocene deposits (unit S2) on top of CGA2 and are lacking on top of CGA1. On the eastern flank of CGA2, sub-unit S1c reflectors onlap and climb above an erosional cliff carved within Lower-Middle Pliocene (unit 2) deposits. The Lower Pleistocene sediments (sub-unit S1b) overlies para-conformably Lower-Middle Pliocene deposits on CGA2 and disconformably Upper Pliocene-Lower Pleistocene deposits (sub-unit S1c) on CGA1 (Figs. 9a, 9b). Although at a lesser amount compared to older units, reflectors of the lower part of S1c appears gently folded by the growth of the anticlines.

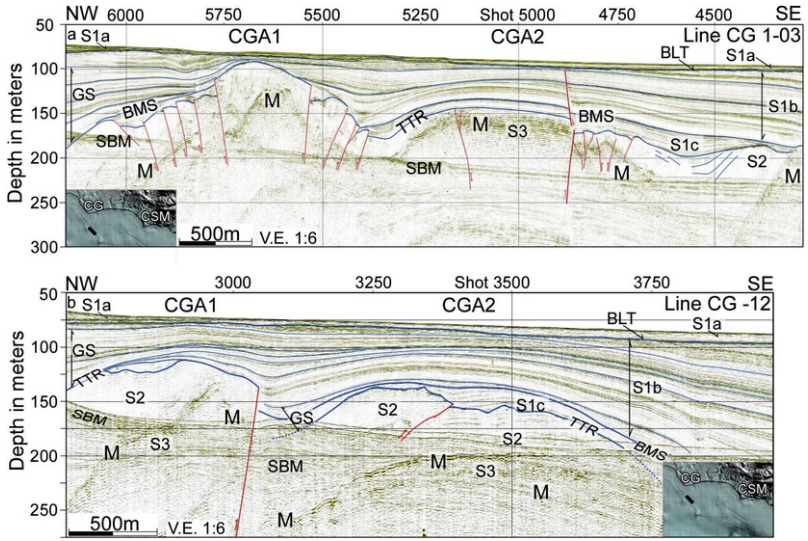

Fig. 9

alt-text: Fig. 9

High-angle faults that have a reverse component of displacement bound the two anticlines. However, only the eastern fault that limits the more structurally elevated CGA1 can be traced with confidence (Fig. 9a). These faults are regarded as minor features when compared to the two major faults that bound the high~~, and they are beyond the resolution of MCS profiles (Fig. 8a, b)~~.

~~4.3.~~4.3 Sciacca Fault system

The NNE-SSW trending SFS extends for a length of ~50 km and a width of ~8 km offshore Capo S. Marco (Fig. 7; Tab~~.~~le 2). The fault array is composed of a sub-rectilinear master fault (SF1) on the west and more curvilinear, east-displacing splay faults on the east, which have ~10 to ~20 km average length. In the north, underneath the shelf, fault SF1 and the splay faults are tighter spaced. In the south, the fault belt runs along a submarine plateau and borders the Nerita Bank. South of the Terrible Bank, structures associated with the SFS are less evident, and the bathymetric expression appears controlled by normal faults related to rifting in the Sicily Channel (Figs. 2; 7; Civile et al., 2018).

MCS profiles crossing the SFS image a shallow antiformal culmination, the Sciacca Anticline (SA; Figs. 7, 10a, b). The fold is bound by faults that flatten upward and converge at depth into sub-vertical fault SF1. This structural association, with a stem fault beneath and outward-branching splay faults that bound a tight fold represents a positive flower structure formed in a strike-slip tectonic environment.

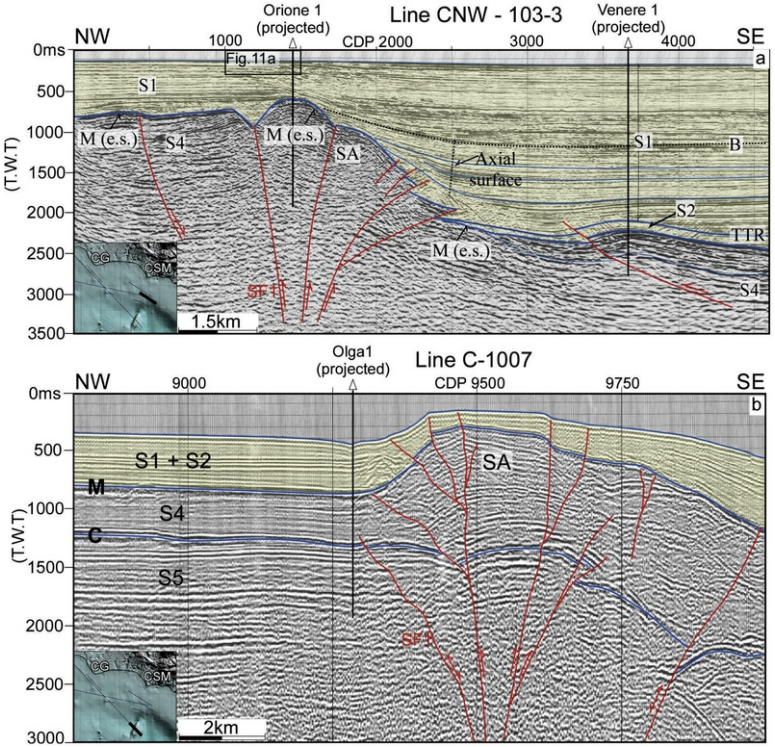

Fig. 10

alt-text: Fig. 10

Change of lateral thickness in Tortonian-Lower Messinian (unit S4) deposits indicates that a component of extensional displacement was accommodated along the SFS during Tortonian-Early Messinian. Indeed, in the southern profile crossing the Nerita Bank (Fig. 7), the thickness of S4 varies from a rather constant value of ~400 ms (~540 m), a value consistent with the ~450 m thickness logged in the Olga 1 well) west of the SFS, to ~1050 ms (~1400 m) in the high and to ~1350 ms (~1800 m) in the eastern flank (Fig. 10b).

Similar information can be gathered from the northern profile crossing the Sciacca shelf. Here, although S3 lacks on the high and older Miocene formations are logged by Orione well beneath the Pleistocene sequence (Fig. 4), S4 reaches a thickness of ~250 m (cf. Venere well, Fig. 4) in the basin east of the fault zone (Fig. 8a). These relations suggest that the SFS was an ~east-directed extensional half-graben during the Late Miocene.

In the northern profile, horizon M is an erosional surface both on the flanks and on the top of the high, as indicated by its unconformable geometry with underlying reflectors and by well-logs (Figs. 4, 10a). The presence of an erosional surface suggests that the previous extensional basin was levelled during Late Messinian, giving a maximum age for tectonic inversion. Deposition of Pliocene-Quaternary sediments up to ~2300 m thick (Figs. 4, 10a) occurred east of the high because of transpressional inversion, which was particularly intense during the Early Pliocene. Growth of the positive structure, whose top remained emergent, continued during deposition of the lower part of S1 up to marker B (dotted line in Fig. 10a). Subsequently, deformation strongly reduced or was overwhelmed by sedimentation that levelled the previous bathymetric differences.

Toward the south, the seismic line C-1007 suggests that the structure continued growing during the Pliocene and likely part of the Quaternary, creating an antiform emerging at the seafloor (Fig. 10b). The difference between the northern (Sciacca shelf) and southern (Nerita Bank) sectors can be partly explained by the proximity of the coast and larger sediment supply availability in the north, which account for the higher thickness of S1 there. In the Terribile bank, the fold broadens and looses structural relief (Fig. 7).

SCS profiles show that folding involves S1b reflectors up to the BLT surface (Figs. 11a). The shallow fold is represented by a broad anticline flexure with a steeply dipping eastern limb, whereas the western limb is shallowly dipping. The eastern limb is cut by several high-angle faults each causing a ~1–2 m extensional offset of the surface BLT and overlying S1a. Additional extensional faults are imaged on top of the anticline, where they form a low-offset

(~3.6 m) crestal graben associated with folding (Fig. 11b). These normal faults are regarded as minor structures associated with folding as often observed in seismic profiles (e.g., Ridente and Trincardi, 2006).

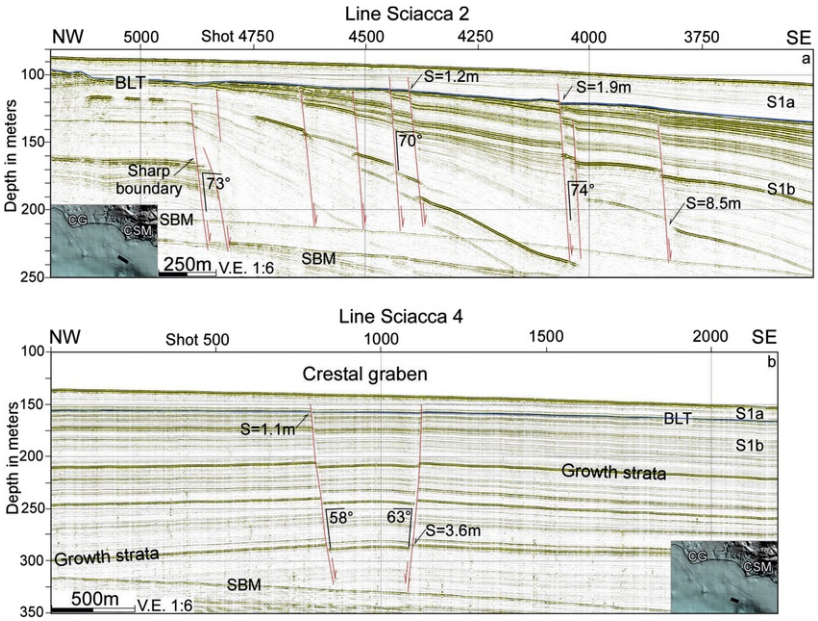

Fig. 11

alt-text: Fig. 11

Based on SCS profiles analysis, the shallow trace of the Sciacca Anticline has an NNE-SSW trend parallel to the main anticline and can be traced for ~16 km offshore Capo S. Marco near Sciacca (SA-N/a and SA-N/b, Fig. 7).

~~5.~~5 Discussion

~~5.1.~~5.1 Structural evolution of foreland faults offshore southwest sicily

Correlation between features detected in the shallowest sub-bottom and at greater depths is pivotal to achieve detailed information on the structural evolution of foreland faults offshore southwest Sicily. To this end, joint analysis of MCS and SCS profiles nicely brackets the history of folding and faulting as revealed by unconformities and growth geometries of *syn*-tectonic strata both on the flanks and on the top of the major transpressional structures.

Interpretation of MCS reflection profiles allows reconstructing a progressive history of transpressional deformation superposed on early extension both for the CGFS and the SFS. Extension occurred during deposition of the Terravecchia Formation (unit S4), which fills the Tortonian to Early Messinian foredeep of the SFTB. At that time, the proximal parts of the foreland were stretched possibly in relation to foreland flexure beneath the advancing SFTB.

Tectonic inversion of the Mid-Late Miocene basins that presently core the CGA and SA likely started in the latest Miocene (Ghisetti et al., 2009; Civile et al., 2018~~),~~). possibly during the Messinian salinity crisis or soon after. This is documented by development of a Late Messinian erosional surface on top of some highs, implying that they stood above the surrounding sea-floor. A significant Latest Messinian-Early Pleistocene shortening component is documented by the uplift of horizon M in the inverted basins and by thickness variations in units S2 and S1c in MCS and SCS profiles (Figs. 8a, ~~8~~b, 9a, b, 10a, b).

Our high-resolution images support the proposal of Fedorik et al. (2017) and Civile et al. (2018) that the CGFS mostly grew during the Pliocene. During the Pliocene, the top of the CGA likely consisted of small seamounts floored by the fold culminations and locally by thrust imbricates. Syn-sedimentary deformation caused the development of erosional surfaces in unit S2, which were onlapped by reflectors of sub-unit S1c (Figs. 9a, ~~9~~b). Erosion possibly occurred in sub-aerial conditions that were enhanced by a Middle-Late Pliocene global sea-level fall (Lisiecki and Raymo, 2005).

According to Fedorik et al. (2017), the CGFS appears sealed by the upper part of the Pliocene-Quaternary succession. By contrast, SCS images presented here reveal that S1c reflectors show thickness changes and growth strata on the limbs of both CGA1 and CGA2 (Figs. 9a, b), which indicates that the two folds continued growing during Latest Pliocene-Earliest Pleistocene. Onland, the Piacenzian-Gelasian (Upper Pliocene-Lower Pleistocene) Belice marly-

arenaceous formation, which is age-correlative of S1c, shows similar growth relations on the flanks of major bedrock folds around the Belice valley area (Mascle, 1979; Monaco et al., 1996; Vitale, 1997). Also, SCS profiles offer evidence that folding and growth strata are well developed in the lower section of sub-unit S1b (Fig~~s~~. 9a, ~~9~~b). These reflectors are correlative to the Lower Pleistocene Marsala Synthem deposits, supporting the notion that the CGFS is active (Civile et al., 2018).

Although tectonic inversion of the Miocene basins along the CGFS progressed during the entire Pliocene-Pleistocene, the resulting positive structure is characterized by faults that retain net extension at depth and show net contraction associated with anticline growth in the upper part (Fig~~s~~. 8a, ~~8~~b). Such feature indicates partial structural inversion of faults, along which the contractional movements did not balance the previous extensional slip (Williams et al., 1989). Furthermore, the geometry of syntectonic strata related to both major (CGA) and minor (CGA1, CGA2) folds suggests a sedimentation rate that outpaces the rate of crestal uplift, resulting in an overlap model of fold growth (Burbank and Vergés, 1994).

To the east, the SFS was considered a transpressional structure that is active along its southern part but is covered by an undeformed Upper Pliocene-Quaternary succession in the northern part (Fedorik et al., 2017). Analysis of high-resolution CHIRP profiles allowed Civile et al. (2018) to argue that the SFS is active along its whole length. The high-resolution SCS profiles for the northern part of the SA confirm that deformation involves the most recent sediments and the sea-floor as well (Fig. 11b).

The continued sedimentation of S1b on the crest of a growing anticline suggests an overlap model (Burbank et al., 1996) for the northern sector of the SFS. Conversely, in the south, around the Nerita Bank (Figs. 7, 10b), fold growth rates overcome the sedimentation rate.

~~5.2.~~5.2 Quantitative analysis of deformation

~~*5.2.1.*~~*5.2.1* *Long-term displacement pattern*

To evaluate the amount of post-Miocene tectonic inversion we measured and compared ~~the offset across faults and~~ the amplitude of folding of horizon M in all seismic profiles crossing the two fault systems. In each profile, we measured the fold amplitude concerning the M horizon by taking the distance from the anticlinal hinge on the high to the synclinal hinge in the adjacent basin (the deepest between the two basins flanking the high).

We then plotted single values of ~~fault offset (for the CGFS) and~~ fold amplitude (for both fault systems) with respect to the distance from the coast of each seismic line imaging the analysed structure. This graph allows to seek for longitudinal variations in displacement of horizon M that provide information on the geometry and size of tectonic structures.

We are aware of the possibility that the differing nature (erosive or depositional) of horizon M on the highs and in adjoining basins carries uncertainty in displacement estimation. Nevertheless, the uncertainty chiefly applies to the case that the horizon M is an erosional surface in the high and grades to evaporitic deposits in the basin, suggesting the existence of a high possibly connected to the Messinian eustatic regression rather than to tectonics. In this context, the tectonic offset may be overestimated if the high continued growing whereas, on the contrary, this value can be underestimated if the basin was inverted. In the case that horizon M marks an erosional surface on the highs and in the basins, and assuming a sub-horizontal attitude of the surface before folding, the estimation is less uncertain.

~~As regards faults, CGF1 and CGF2, the longitudinal distribution of offset measurements depicts broadly symmetric bell-shaped curves (Fig. 12a). The maximum displacement of horizon M (~ 250 m) is recorded in the central part of the two faults at ~ 20 km from the coast and decreases to minimum values of ~ 50 m to both ends. This distribution indicates that the faults were almost entirely sampled by the available profiles along their length. The lateral terminations of the curves where displacement values tend to zero highlight the location of fault tips. The bell-shaped geometry that displays the greatest displacement near the centre of the faults and steadily decreases toward the fault tips is consistent with the characteristic displacement model for faults (Cowie and Scholz, 1992).~~

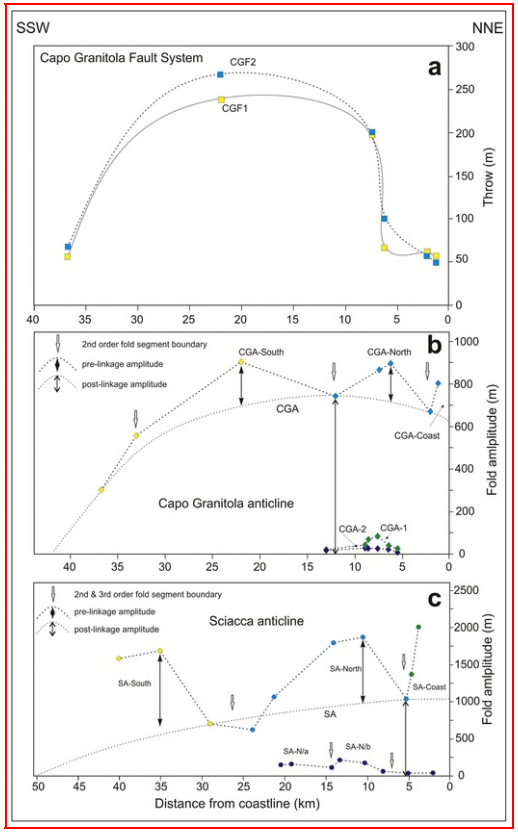

Fig. 12

alt-text: Fig. 12

~~The scaled distance between the fault tips, which represents the fault trace length (Kim and Sanderson, 2005), is is ~35 km for both CGF1 and CGF2. The non-zero displacement at fault tips suggests that the two faults continue of few (<5) km on both the north-east and south-west sides. Summarising, based on the displacement model, we estimate a maximum ~45 km length for the faults (Table 2), in good agreement with previous estimation by Civile et al. (2018).~~

The fold amplitude distribution for the Capo Granitola Anticline (CGA), measured with respect to the basins to the east and west (in the south) has two maxima (~0.9 km) at 6 and ~~22~~37 km off the coast, respectively. These maxima ~~define~~ describeas many undulations which define 2nd order folds along the structural high (CGA-North and CGA-South, Figs. 7, 12~~b~~a; Tab~~.~~le 2). A truncated maximum (~~0.8~~ ~1 km) is observed approaching the coast (CGA-Coast), possibly reflecting an under-sampled continuation of the anticline to the north or the activity of the on-shore Castelvetrano segment of the ATF (Fig. 2). The ~~curve has a truncated southern end (0.3 km amplitude) at 37 km, but a~~ southward projection of the curve to the intersection with the null displacement axis indicates the fold extends over 40 km off the coast (Tab~~.~~le 2). The estimated length is well consistent with the size of bounding faults CGF1 and CGF2 (Fig. 7), supporting the notion of a linked growth of faults and fold.

The curve for the Sciacca Anticline (SA) was constructed by measuring the amplitude with respect to the basin in the east, which represents by far the deeper structural depression (Figs. 2, 10a). The origin of this deep basin is supposed to be linked to the transpressional displacement on the SF. However, a component of subsidence related to extensional flexure of the foreland underneath the advancing Gela Nappe (Fig. 2) cannot be discarded. Thus, we regard our estimates as maximum bounds for growth of the SA.

The curve is characterized by a ~~gentle~~ net south-westward decrease of the amplitude modulated by two bell-shaped undulations with maximum values of 1.~~85~~9 and 1.~~7~~1 km at an ~1~~1~~4 and ~~35~~29 km distance from the coast, respectively. These undulations define 2nd order folds (SA-N and SA-S, Figs. 7, 12~~e~~b; Tab~~.~~le 2). The northern fold (SA- North) has a length of 1~~8~~7 km and is located under the shelf and slope. The southern fold (SA-South), has a sampled length of 1~~5~~4 km centred on the Nerita Bank, ~~but the projection of its southern tips indicates that it may extend~~and an additional fold segment can be present further south in the Terrible Bank for a ~~total~~ length of >~~20~~5 km. An additional under-sampled curve is observed close to the coast (SA-

Coast, Fig. 12eb); ~~and exhibits a truncated maximum value of 2 km~~. As for the Capo Granitola Anticline, the presence of SA-Coast may be related either to a northward continuation of the SFS behind the coastline or to uplift related to the activity of the front of the SFTB near Sciacca (Fig. 2).

~~5.2.2.~~5.2.2 *Short-term displacement pattern*

Analysis of SCS profiles provides geometrical parameters for shallower structures, which give information about recent and current pattern of deformation. This analysis allows estimating the trace length of structures at a smaller spatial scale and at a shorter time scale. The almost regular ~1 km spacing between profiles provides a homogenous distribution of value estimates. Computation of fold amplitudes, however, is affected by errors residing in the likely original non-planar deposition of Quaternary sediments above already existing structural highs. For this reason, we regard our estimates as maximum bounds.

Three minor anticline folds are developed on top of the northern part of the Capo Granitola anticline (Fig. 8a), but our SCS profile grid sufficiently samples only two of them (CGA1, CGA2). These anticlines represent 3rd order folds in the structural architecture (Tab.le 2). Fig~~ures~~. 13a and b display the amplitude pattern of reflector Base of Marsala Synthem (BMS) along CGA1 and CGA2. The trend for CGA1 exhibits a complete fold geometry with a slightly asymmetric, ~80 m high central peak. Using an adjusted profile (dashed shape calculated from a 2nd order polynomial regression), the resulting fold amplitude is approximated to a bell-shape (dotted line in Fig. 13a). This geometry reveals that the structure is almost fully detected by the crossing seismic lines, with a minimum trace length of 7.5 km. Conversely, CGA2 presents a partly complete curve with an asymmetric, ~30 m high central peak (Fig. 13b). Based on the adjusted profile (dotted line, Fig. 13b), we estimate a ˜10 km length for CGA2 (Tab.le 2).

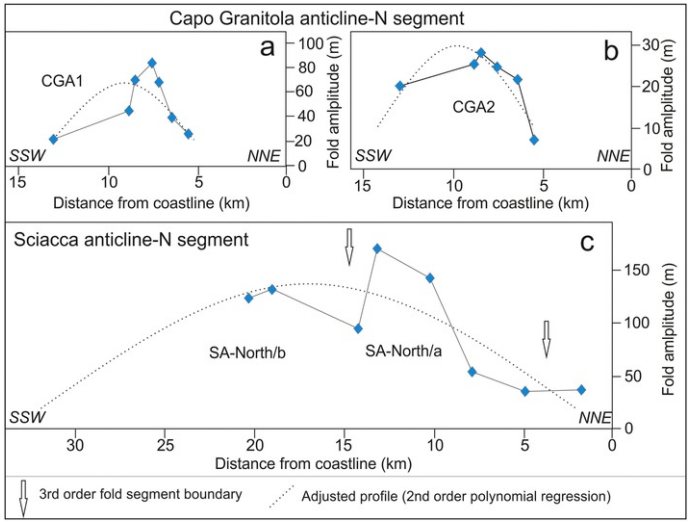

Fig. 13

alt-text: Fig. 13

The BMS horizon is not identified in the northern part of the Sciacca Anticline. Thus, we measured the longitudinal changes in fold amplitude based on the horizon Top of Marsala Synthem (TMS). The shallow fold imaged by SCS profiles shows a maximum amplitude (~200 m) at ~13 km from the coast (Fig. 13c). The plot shows two culminations highlighting the presence of two minor folds (SA-North/a and SA-North/b; Fig. 13c, Tab.le 2), the first of which is not entirely detected as suggested by its incomplete shape. These shallow folds represent 3rd order folds concerning the crustal structure mapped using MCS profiles. The trace length of the combined SA-North/a and SA-North/b is ~20 km, and we estimate a total length of ~30 km using the adjusted profile (Fig. 13c). The length estimate is consistent with the trace length of the crustal-scale fold SA-North, and the position of the maximum amplitude for the long- and short-term curve coincide (Fig. 12~~b~~a).

~~5.3.~~5.3 Fold growth, fault segmentation and structural linkage

Fig~~ures~~. 12~~b~~a and ~~e~~b highlights that the 2nd order northern and southern folds that compose the CGA and SA have bell-shaped longitudinal profiles, and thus represent distinct structures. Based on the spatial correspondence between individual folds and adjoining faults, we suggest that the northern and southern parts of the CGFS and SFS are composed by individual fault segments (Fig. 7). In this reconstruction, the lateral change in fold amplitude allows to estimate the corresponding variation in deformation accommodated on the related fault segments and to search for the position of segment boundaries. We take the minimum inflection points between two curves as the locus of

separation between as many adjoining fault segments (Fig. 12a, b). The map position of fault segment boundaries derived from fold analysis is consistent with changes in orientation and spacing of fault arrays in both the CGFS and SFS (Fig. 7).

Detailed inspection of the fold amplitude curves provides Information about the growth history of the transpressional folds and related fault segments. Indeed, the long-term curve for horizon M shows that the 2nd order folds lie above the amplitude value of the larger fold. This observation suggests that the 2nd order folds have grown separately of ~~170~~300–~~19~~400 m (Capo Granitola Anticline) and ~~8~~500–~~98~~1100 m (Sciacca Anticline), as estimated from the difference between their maximum amplitude and the height of the intervening saddle (Fig~~s~~. 12~~b~~a, ~~12~~eb; Tab~~.~~le 2). Afterword, the 2nd order folds within both fault systems have joined to form a single, 1st order growing fold.

The reconstructed fold evolution likely mirrors the growth and linkage history of underlying fault segments, which we argue have slipped separately in the early part of their history of tectonic inversion. Later, the fault segments in both systems have probably linked to produce a single deformation profile (Cowie and Scholz, 1992).

A similar reconstruction can be proposed for the recent (~1 Ma) evolution of the northern part of the Sciacca Anticline, which consists of two 3rd order folds, SF-North/a and SF-North/b (Fig. 13c; Tab~~.~~le 2). We regard the two minor folds as being grown separately until they accrued a vertical displacement of 50 (SF-North/a) and 100 m (SF-North/b), as estimated from the height difference between their maximum amplitude and the height of the saddle between them. Afterward, the fault segments underlying the two 3rd order folds have probably joined with an additional 60–70 m vertical displacement accommodated by the linked structure. However, the fault segments underlying these minor folds in the Quaternary represent smaller scale structures that are not resolved by MCS profiles.

In addition, by comparing the along-strike displacement pattern for the two time-windows provided by horizons M (~5.3 Ma) and BMS-TMS (~1 Ma), it appears that the shape of the amplitude change profile persist through time for the northern portions of the Capo Granitola and Sciacca anticlines (Fig~~s~~. 12~~b~~a, ~~e~~b).

~~5.4.~~5.4 Comparison of long-term and short-term fold growth rates

Results of the previous section indicate that, based on their geometry, position and growth history, the deeper and shallower folds detected in MCS and SCS profiles in the northern sector of the CGFS and SFS spatially coincide and are the expression of the same structure at diverse time-windows. By consequence, understanding whether deformation accommodated at different time-scales followed a linear evolution or was characterized by discrete pulses of activity offers the opportunity to gain insights on the more general issue of the mechanic behaviour of faults.

To this end, we reconstructed the fold growth history using horizons representative of the long- (horizon M) and short-term (horizons BMS and TMS) tectonics. We used maximum amplitudes derived from the northern segments of the Capo Granitola and Sciacca anticlines, where deformation marker horizons are available from both MCS and SCS profiles (Figs. 7, 12b, c). We also evaluate the total deformation accommodated on the southern segments of the two anticlines where there are no SCS information, and thus the comparison is not possible. Nevertheless, the estimate of fold growth rates in the south provide long-term values against which compare the time-incremental values computed for the northern segments.

As discussed in Section 5.1, much of fold growth offshore Capo Granitola and Sciacca occurred during the latest Miocene-Pliocene. For this reason, we computed the long-term maximum incremental fold uplift between horizon M (5.3 Ma) and the top of the Belice Marnoso-Arenacea (1.8 Ma), which broadly marks the end of growth strata in MCS profiles (Figs. 8c, 10a). Although there is evidence that fold growth commenced locally since the Late Messinian (~6 Ma), we assume an average 5.3 Ma age for onset of transpression. Then, we used the long-term rate computed on M to extrapolate forward the fold amplitude accrued until 1.8 Ma (incremental fold amplitude, Tab~~.~~le 3).

Table (I would like to slightly modify the Table but I was not able to do it in the proofcentral system. I upload the revised Table 3)3 Maximum fold growth rates for the Capo Granitola and Sciacca folds. See text for details.

alt-text: Table 3

1st order fold	2nd & 3rd order fold	Horizon	Incremental deformation age (ka)	Total fold amplitude (m)	Incremental fold amplitude (m)	Fold growth rate (mm/yr)	Time-span
Capo Granitola Anticline	CGA1-2	BMS	1100-0	80	80	0.07	Short-term
	CGA-North	M	5332–1801 = 3531	900	774	0.22	Long-term
	CGA-South	M	5332–1801 = 3531	906	906	0.17	Total
Sciacca anticline	SA-N/b	TMS	780–0	170	170	0.22	Short-term
	SA-North	M	5332–1801 = 3531	1933	1537	0.44	Long-term
	SA-South	M	5332–1801 = 3531	1680	1680	0.32	Total

For the short-term deformation, we used the maximum amplitude of folds CGA1-CGA2 and SA-North/b measured in SCS profiles on horizons BMS (1.1 Ma) and TMS (0.78 Ma), respectively (Tab~~.~~le 3). We chose horizon TMS instead of BMS for fold SA-b because the bottom of sub-unit S1b is not imaged in SCS profiles of the Sciacca system (Fig. 11b). We assume, based on evidence from SCS images that this second deformation stage lasts until the present.

Using the incremental fold amplitudes between the picked horizons, we computed the growth rates for the time intervals 5.3~~-~~–1.8 and 1.8~~-~~–0 Ma (Fig. 14; Tab~~.~~le 3). Results illustrate that the northern Capo Granitola anticline grow at relatively high-rate (0.22 mm/yr) during the older time interval, and much slower (0.07 mm/yr) afterward (Fig. 14). Similarly, growth rates for the Sciacca anticline were higher during the Pliocene-Early Pleistocene (0.44 mm/yr), and halved during the last 1.8 Ma.

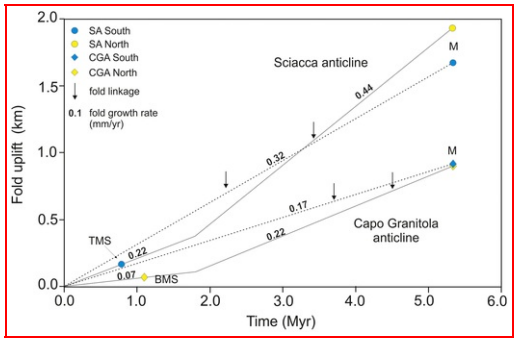

Fig. 14

alt-text: Fig. 14

For the southern sector of the Capo Granitola and Sciacca anticlines only the total uplift and relative rate (0.1~~7~~9 and 0.~~3~~20 mm/yr, respectively) are shown in Fig~~ure~~. 14. Based on the observation that the southern part of the SA exhibits a bathymetric expression of deformation (Fig. 10b), it is possible that the growth rate of this anticline did not change through time. The fold uplift rates estimated for the Sciacca Anticline ~~but~~ both at long- and short-term are twice those computed for the Capo Granitola Anticline.

Because we did not apply decompaction correction for seismic units, we estimate that the rates estimated from measured amplitudes are ~50% above their real value (e.g. Laubach et al., 2000; Maesano et al., 2013).

Finally, we estimated the timing of linkage between individual folds at the sub-segment scale. By using the amplitude of the 2nd order (pre-linkage) folds (Tab~~.~~le 2), we calculated the predicted time of linkage (arrows in Fig. 14). We made two estimates for each anticline. For the CGA, estimates vary between ~~4~~3.4~~-5-~~ and 3.~~7~~8 Ma, whereas the linkage age estimates for the SA are younger (~~3.4-~~–2.~~2~~7 Ma). Although further refinements are not possible with available data, we suggest the timing of linkage signals the ensuing end of fast fold growth.

~~5.5.~~5.5 Regional tectonic context of foreland transpression

The tectonic inversion recorded on the CGFS and SFS in the Pelagian foreland since the end of the Miocene is linked to the regional tectonic evolution of this sector of the central Mediterranean area. In western-central Sicily, geological and geophysical studies document that the Trapanese and Saccense foreland, previously underthrust beneath the SFTB, was involved in shortening along steep transpressional ramps starting from Late Miocene as well (Avellone et al., 2010). In southwest Sicily (Sicani Mountains), this switch occurred later, after deposition of the Trubi Formation (Catalano et al., 2000; Avellone et al., 2010). Whether the deep-seated faults detached at the interface between the crystalline basement and the sedimentary succession (Catalano et al., 2002; Avellone et al., 2010) or emanated from the basement is not yet resolved. Nevertheless, it is generally acknowledged that reverse and transpressional motion reactivated earlier structures inherited from the Mesozoic rifting (Catalano, 1982; Oldow et al., 1990; Renda et al., 2000).

Offshore southwest Sicily, the foreland transpressional faults are thought to be inherited Mesozoic normal faults that were subsequently reactivated in basement-involved deformation (Argnani et al., 1986; Ghisetti et al., 2009; Civile et al., 2018). The faults that we mapped have relatively high dip-angles (~60°~~-~~–~80°) and represent shallow splays of the deep-seated faults.

The causes for the switch from thin- to thick-skinned shortening beneath the SFTB are not fully understood. However, the evidence that broadly coeval deep-seated reverse and transpressional faults were active both in the western Sicily SFTB (Oldow et al., 1990; Avellone et al., 2010) and in its foreland highlights that the effects of the continental collision were transmitted far beneath the thrust belt to the pre-fractured foreland domain. Indeed, the left-oblique kinematics of the CGFS and SFS is consistent with the last ~10 Ma regional plate convergence reconstructed by tectonic models and presently documented by geodesy and seismicity (Fig. 1). The convergence is the primary

controlling process for both thrust belt development and foreland transpression.

As noted previously (e.g. Ghisetti et al., 2009; Avellone et al., 2010), the switch to the deep-seated deformation was likely triggered by involvement of stiff platform carbonates in continental collision. Within the Saccense foreland, during deposition of Tortonian-Early Messinian sequence S4, the inherited ~N-S striking faults were active as normal or transtensional and accommodated flexure of the foreland beneath the still remote thrust belt. ~~In~~ Since latest Miocene-Early Pliocene, when the orogenic wave indented thicker sections of the Pelagian foreland such as the Saccense and Hyblean domains, these sectors acted to buttress further advancement of the SFTB (Ghisetti et al., 2009). In this context, transpressional inversion of the foreland faults in the Sicily Channel and in southern Sicily served to convey more rapid migration of the Gela Nappe between the Saccense and Hyblean sectors (Fig. 1).

A possible link between the regional tectonic frame and the behavior of studied faults is offered by the observed change in fold growth rate during the last ~5.3 Ma (Fig. 14). Based on the conceptual model of deformation reconstructed in this work, with the folds being expression of motion of underlying blind transpressional faults, the estimate of fold uplift rate can be taken as a proxy for the vertical slip-rate on the underlying blind faults. In this scenario, the transpressional reactivation of foreland faults since the end of the Miocene could mark the approaching of the thick-skinned thrust belt around both sides of the Saccense foreland indenter (Figs. 1, 2).

We further suggest that the overall southern dip of long-term fold amplitude profiles (Fig~~s~~. 12a, b) records the impingement of the thrust system onto the Saccense foreland domain. Based on the age estimate of linkage (~~broadly 2.5-4.5 Ma~~~2.7 Ma for the Sciacca anticline), we argue that linkage could have been triggered by involvement of the Saccense domain in thick-skinned deformation, which in southwest Sicily (Catalano et al., 2000) is dated after deposition of the Trubi Formation (~3.1 Ma). This occurrence may have heralded the ensuing reduction in rates, which persist today.

~~6.~~6 Conclusions

Integration of high-penetration MCS and high-resolution SCS reflection profiles allowed to document that the upper crustal (~5 km) and near sea-bottom (~200~~-~~–300 m) folds and faults imaged offshore Capo Granitola and Sciacca are different scale expression of two regional transcurrent fault systems, the CGFS and SFS, that dissect the Pelagian foreland of the Sicilian orogenic belt. The two systems were active in left transpression since the Latest Miocene-Early Pliocene and are still active. Transpressional deformation along the CGFS and SFS inverted previous extensional or transtensional basins that developed during Late Tortonian-Early Messinian (Late Miocene).

Transpressional deformation is expressed by push-up folds that are organized in 1st, 2nd and 3rd order structures. The fold amplitude of long- (5.3 Ma) and short-term (1.1 Ma) horizons show systematic along-strike changes with 2nd and 3rd order undulations, respectively that approximate bell-shaped anticlines. The 2nd order undulations indicate that these secondary folds, and by inference the underlying blind transpressional faults, are composed of two distinct segments, northern and southern. Estimate of displacement and analysis of growth strata document that the folds and related fault segments have grown separately for the early part of their history, until they became linked between ~~3~~2.7 (SA) and ~~4~~3.4-3.8 (CGA) Ma. Fold growth rates were high in the Pliocene and reduced ~~since~~ in the Early Pleistocene.

The onset of foreland transpression is broadly coeval to the transition from thin-skin to deep-seated thrusting and transpression in the Sicilian thrust belt. On this basis, we conclude that both processes are related to impingement of continental collision onto stiff portions of the continental margin that transmitted stresses related to convergence far into the Pelagian foreland. Involvement of the foreland in deformation triggered by deep-seated thrusting may be related to fold segments linkage between ~3~~-~~–4 Ma. Long-lasting transpression supports the notion that the foreland block is strongly fractured, with inherited shear zones focusing the locus of strain in the regional convergence context.

Uncited references (The uncited references are in the Figure captions)

Argnani et al., 1987

Bigi et al., 1989

Meccariello et al., 2017

Pepe et al., 2010

~~Ryan et al., 2009~~

Acknowledgements

The work benefits by grants of University of Palermo in the frame of the project “Earthquake Potential of Active Faults using offshore Geological and Morphological Indicators”, and of the University of Catania in the frame of the project “Multidisciplinary analysis of the deformation in the around of active tectonic structures (responsible G. Barreca)”. This work is part of Melania Meccariello~~’~~s PhD thesis at the University of Naples Federico II. We thank Alfonso Analfino for his assistance during the seismic data acquisition onboard the R/V Neptune 1. The authors would also like to thank Eni E&P for having provided us multi-channel

seismic reflection profiles and for having permitted the publishing of a seismic line. We acknowledge the careful reviews of A. Billi and S. Dominguez that greatly helped to improve the manuscript.

The bathymetric metadata and Digital Terrain Model data products have been derived from the EMODnet Bathymetry portal - http://www.emodnet-bathymetry.eu.

References

Antonelli M., Franciosi R., Pezzi G., Querci A., Ronco ~~G. P.~~G.P. and Vezzani F., Paleogeographic evolution and structural setting of the northern side of the Sicily Channel, *Mem. Soc. Geol. It.* **41** (1), 1988, 141–157.

Argnani A., The Gela Nappe: ~~E~~evidence of accretionary melange in the Maghrebian foredeep of Sicily, *Mem. Soc. Geol. It* **38**, 1987, 419–428.

Argnani A., Neogene basins in the Strait of Sicily (Central Mediterranean): ~~t~~Tectonic settings and geodynamic implications, In: Boschi ~~E~~E., et al., (Eds.), *Recent ~~e~~Evolution and ~~s~~Seismicity of the Mediterranean ~~r~~Region,* 1993, Kluwer Academic Publication; Dordrecht, 173–187.

Argnani A., Cornini S., Torelli L. and Zitellini N., Neogene-Quaternary foredeep system in the Strait of Sicily, *Mem. Soc. Geol. It.* **36**, 1986, 123–130.

Argnani A., Cornini S., Torelli L. and Zitellini N., Diachronous foredeep-system in the Neogene-Quaternary of the Strait of Sicily, *Mem. Soc. Geol. It* **38**, 1987, 407–417.

Avellone G., Barchi ~~M. R.~~M.R., Catalano R., Gasparo Morticelli M. and Sulli A., Interference between shallow and deep-seated structures in the Sicilian fold and thrust belt, Italy, *~~Journal of the Geological Society~~J. Geol. Soc.* **167**, 2010, 109–126.

Barreca G., Bruno V., Cocorullo C., Cultrera F., Ferranti L., Guglielmino F., Guzzetta L., Mattia M., Monaco C. and Pepe F., Geodetic and geological evidence of active tectonics in south-western Sicily (Italy), *~~Journal of Geodynamics~~J. Geodyn.* **82**, 2014, 138–149.

Basilone L., Litostratigrafia della Sicilia, 2012, Dipartimento di Scienze della Terra e del Mare - Università degli Studi di Palermo; Palermo.

Bigi G., Castellarin A., Catalano R., Coli M., Cosentino D., Dal Piaz G.V., Lentini F., Parotto M., Patacca E., Praturlon A., Salvini F., Sartori R., Scandone P. and Vai G.B., Synthetic ~~s~~Structural-~~k~~Kinematic ~~m~~Map of Italy, ~~s~~Scale 1:2.000.000, 1989, CNR, Progetto Finalizzato Geodinamica; Roma.

Burbank ~~D. W.~~D.W. and Vergés J., Reconstruction of topography and related depositional systems during active thrusting, *J. Geophys. Res. Solid Earth* **99** (B10), 1994, 20281–20297.

Burbank D., Meigs A. and Brozović N., Interactions of growing folds and coeval depositional systems, *~~Basin Research~~Basin Res.* **8** (3), 1996, 199–223.

Calò M. and Parisi L., Evidences of a lithospheric fault zone in the Sicily Channel continental rift (southern Italy) from instrumental seismicity data, *Geophys. J. Int.* **199** (1), 2014, 219–225.

Catalano, R., D~~'~~'Argenio, B., 1982. Schema Geologico della Sicilia. In: Catalano, R. & D~~'~~'Argenio, B. (Eds.) Guida alla geologia della Sicilia occidentale. Memorie della Società Geologica Italiana, ~~XXIV (Suppl. A)~~vol. XXIV (Suppl. A), 9–41.

Catalano R., Franchino A., Merlini S. and Sulli A., Central western Sicily structural setting interpreted from seismic reflection profiles, *Mem. Soc. Geol. It.* **55**, 2000, 5–16.

Catalano R., Merlini S. and Sulli A., The structure of western Sicily, central Mediterranean, *Pet. Geosci.* **8**, 2002, 7–18.

Catalano R., Valenti V., Albanese C., Accaino F., Sulli A., Tinivella U., Gasparo Morticelli M., Zanolla C. and Giustiniani M., Sicily~~'~~'s fold–thrust belt and slab roll-back: the SI. RI. PRO. ~~s~~Seismic crustal transect, *~~Journal of the Geological Society~~J. Geol. Soc.* **170** (3), 2013, 451–464.

Cavallaro D., Monaco C., Polonia A., Sulli A. and Di Stefano A., Evidence of positive tectonic inversion in the north-central sector of the Sicily Channel (Central Mediterranean), *~~Nat. Hazards.~~Nat. Hazards* **86**, 2017, S233–S251, https://doi.org/10.1007/s11069-016-2515-6.

Civile D., Lodolo E., Alp H., Ben-Avraham Z., Cova A., Baradello L., Accettella D., Burca M. and Centonze J., Seismic stratigraphy and structural setting of the Adventure Plateau (Sicily Channel), *~~Marine Geophysical Research~~Mar. Geophys. Res.* **35** (1), 2014, 37–53.

Civile D., Lodolo E., Accaino F., Geletti R., Schiattarella M., Giustiniani M., Fedorik J., Zecchin M. and Zampa L., Capo Granitola-Sciacca Fault Zone (Sicilian Channel, Central Mediterranean): Structure vs magmatism, *~~Marine~~*

~~and Petroleum Geology~~*Mar. Pet. Geol.* 2018, https://doi.org/10.1016/j.marpetgeo.2018.05.016.

Cogan J., Rigo L., Grasso M. and Lerche I., Flexural tectonics of south-eastern Sicily, ~~*Journal of Geodynamics*~~*J. Geodyn.* **11** (3), 1989, 189–204.

Cowie ~~P. A.~~P.A. and Scholz ~~C. H.~~C.H., Displacement-length scaling relationship for faults: data synthesis and discussion, ~~*Journal of Structural Geology*~~*J. Struct. Geol.* **14** (10), 1992, 1149–1156.

DeCelles P.G. and Giles K.A., Foreland basin systems, ~~*Basin Research*~~*Basin Res.* **8**, 1996, 105–123.

Di Maggio C., Madonia G., Vattano M., Agnesi V. and Monteleone S., Geomorphological evolution of western Sicily, Italy, ~~*Geologica Carpathica*~~*Geol. Carpath.* **68** (1), 2017, 80–93.

Di Stefano P., Favara R., Luzio D., Renda P., Cacciatore M.S., Calò M., Napoli G., Parisi L., Todaro S. and Zarcone G., A regional-scale discontinuity in western Sicily revealed by a multidisciplinary approach: ~~A~~a new piece for understanding the geodynamic puzzle of the southern Mediterranean, *Tectonics* **34**, 2015, https://doi.org/10.1002/2014TC003759.

Fedorik J., Toscani G., Lodolo E., Civile D., Bonini L. and Seno S., Structural analysis and Miocene-to-~~P~~present tectonic evolution of a lithospheric-scale, transcurrent lineament: ~~T~~the Sciacca Fault (Sicilian Channel, Central Mediterranean Sea), *Tectonophysics* **722**, 2017, 342–355.

Ferranti, L., Burrato, P., Pepe, F., Santoro, E., Mazzella, M. E., Morelli, D., Passaro, S., Vannucci, G., 2014. An active oblique-contractional belt at the transition between the Southern Apennines and Calabrian Arc: The Amendolara Ridge, Ionian Sea, Italy. Tectonics, 33/11, 2169-2194. DOI: 10.1002/2014TC003624 Finetti I. and Morelli C., Geophysical exploration of the Mediterranean Sea, In: *Osservatorio geofisico sperimentale,* 1973.

Ghisetti ~~F. C.~~F.C., Gorman ~~A. R.~~A.R., Grasso M. and Vezzani L., Imprint of foreland structure on the deformation of a thrust sheet: ~~T~~the Plio-Pleistocene Gela Nappe (southern Sicily, Italy), *Tectonics* **28** (4), 2009.

Grasso M., The Apenninic-Maghrebian orogen in southern Italy, Sicily and adjacent areas, In: Vai ~~GB~~G.B. and Martini ~~IP~~I.P., (Eds.), *Anatomy of an ~~o~~Orogen: ~~t~~The Apennines and ~~a~~Adjacent Mediterranean ~~b~~Basins: Norwell,* 2001, Kluwer Academic Publishers; Massachusetts, 255–286.

Grasso M., Miuccio G., Maniscalco R., Garofalo P., La Manna F. and Stamilla R., Plio-Pleistocene structural evolution of the western margin of the Hyblean plateau and the Maghrebian foredeep, SE Sicily; implications for the deformational history of the Gela Nappe, *Annales Tectonicae* **9**, 1995, 7–21.

~~Kim Y. S.~~Y.S. ~~and Sanderson D. J.~~D.J., ~~The relationship between displacement and length of faults: a review,~~ ~~*Earth-science reviews*~~*Earth Sci. Rev.* ~~**68** (3), 2005, 317–334.~~

Lambeck K., Antonioli F., Anzidei M., Ferranti L., Leoni G., Scicchitano G. and Silenzi S., Sea level change along the Italian coast during the Holocene and projections for the future, ~~*Quaternary International*~~*Quat. Int.* **232** (1~~-~~–2), 2011, 250–257.

Laubach S.E., Schultz-Ela D.D. and Tyler R., Differential compaction of interbedded sandstone and coal, ~~*Geological Society, London, Special Publications*~~*Geol. Soc. Lond., Spec. Publ.* **169**, 2000, 51–60, https://doi.org/10.1144/GSL.SP.2000.169.01.04.

Lickorish W.H., Grasso M., Butler R.W.H., Argnani A. and Maniscalco R., Structural styles and regional tectonic setting of the “Gela Nappe” and frontal part of the Maghrebian thrust belt in Sicily, *Tectonics* **18**, 1999, 655–668.

Lisiecki L.E. and Raymo M.E., A Pliocene-Pleistocene stack of 57 globally distributed benthic D18O records, *Paleoceanography* **20**, 2005, , PA1003https://doi.org/10.1029/2004PA001071.

Maesano F.E., Toscani G., Burrato P., Mirabella F., D~~'~~ambrogi C. and Basili R., Deriving thrust fault slip rates from geological modelling: examples from the Marche coastal and offshore contraction belt, Northern Apennines, Italy, ~~*Marine and Petroleum Geology*~~*Mar. Pet. Geol.* **42**, 2013, 122–134.

Malinverno A., Cafiero M., Ryan ~~W. B. F.~~W.B.F. and Cita ~~M. B~~M.B., Distribution of Messinian sediments and erosional surfaces beneath the Tyrrhenian sea-geodynamic implications, ~~*Oceanologica Acta*~~*Oceanol. Acta* **4** (4), 1981, 489–495.

Mascle G., Ètude géologique des Monti Sicani, *Mem. Riv. It. Paleont. e Strat.* **16**, 1979, 1–431.

Meccariello M., Ferranti L., Barreca G. and Palano M., New insights on the tectonics of the Lampedusa Plateau from the integration of offshore, on-land and space geodetic data, *Ital. J. Geosci.* **136** (2), 2017, 206–219.

Monaco C., Mazzoli S. and Tortorici L., Active thrust tectonics in western Sicily (southern Italy): the 1968 Belice earthquake sequence, *Terra Nova* **8** (4), 1996, 372–381.

Oldow, J. S., Channell, J. E. T., Catalano, R., D~~'~~Argenio, B., 1990. Contemporaneous thrusting and large-scale rotations in the western Sicilian fold and thrust belt. Tectonics, 9, 661–681.

Pepe F., Sulli A., Bertotti G. and Cella F., Architecture and Neogene to recent evolution of the western Calabrian continental margin: an upper plate perspective to the Ionian subduction system, central Mediterranean, *Tectonics* **29**, 2010, 1–24, https://doi.org/10.1029/2009TC002599.

Renda P., Tavarnelli E., Tramutoli M. and Gueguen E., Neogene deformations of Northern Sicily, andtheir implications for the geodynamics of the Southern Tyrrhenian Sea margin, ~~*Memorie Società Geologica Italiana*~~*Mem. Soc. Geol. Ital.* **55**, 2000, 53–59.

Reuther C.D., Ben Avraham Z. and Grasso M., Origin and role of major strike-slip transfers during plate collision in the central Mediterranean, *Terra Nova* **5**, 1993, 249–257.

Ridente D. and Trincardi F., Active foreland deformation evidenced by shallow folds and faults affecting late Quaternary shelf–slope deposits (Adriatic Sea, Italy), ~~*Basin Research*~~*Basin Res.* **18** (2), 2006, 171–188.

~~Ryan W.B.F., Carbotte S.M., Coplan J.O., O'Hara S., Melkonian A., Arko R., Weissel R.A., Ferrini V., Goodwillie A., Nitsche F., Bonczkowski J. and Zemsky R., Global Multi-Resolution Topography synthesis, *Geochem. Geophys. Geosyst.* **10**, 2009, , Q03014https://doi.org/10.1029/2008GC002332.~~

Soumaya A., Ben Ayed N., Delvaux D. and Ghanmi M., Spatial variation of present-day stress field and tectonic regime in Tunisia and surroundings from formal inversion of focal mechanisms: geodynamic implications for central Mediterranean, *Tectonics* **34**, 2015, 1154–1180, https://doi.org/10.1002/2015TC003895.

Vitale F.P., The Belice and Menfi basins: sequence stratigraphy and evolution during the Pliocene and the Early Pleistocene, In: Catalano R., et al., (Eds.), *Field Guidebook: Time ~~s~~Scales and ~~b~~Basin ~~a~~Dynamics. Sicily, the ~~a~~Adjacent Mediterranean and ~~o~~Other ~~n~~Natural ~~l~~Laboratories, 8th Int. Lithos. Prog. ~~w~~Workshop Palermo, Italy* 1997, 48–58.

Williams ~~G. D.~~G.D., Powell ~~C. M.~~C.M. and Cooper ~~M. A.~~M.A., Geometry and kinematics of inversion tectonics, ~~*Geological Society, London, Special Publications*~~*Geol. Soc. Lond., Spec. Publ.* **44** (1), 1989, 3–15.

Highlights

- Seismic reflection profiles evidence tectonic inversion and active strike-slip faults offshore SW Sicily foreland
- Pliocene-Quaternary transpressional inversion of Late Miocene extensional basins developed push-up ridges on blind transcurrent and reverse faults
- Transpressional fold growth rates were high in Latest Miocene-Pliocene and decreased during Quaternary

Queries and Answers

Query:

Please provide caption for Fig. 1.

Answer: Fig. 1 – Main geodynamic features of the central Mediterranean area (partly adapted from **Argnani, 1986**; **Ghisetti et al., 2009; Catalano et al., 2013; Soumaya et al., 2016**). The large arrow shows orientation and rate of the predicted motion of Nubia relative to Eurasia according to MORVEL plate motion model (after **Meccariello et al., 2017**). Water depth in km. The blue dashed rectangle indicates the location of Fig. 2. Labels are as follow: HY, Hyblean Plateau; GN, Gela Nappe; SC, Saccense sector; SFTB, Sicily Fold and Thrust Belt; CGFS, Capo Granitola Fault System; SFS, Sciacca Fault System; SCFS, Scicli Fault System.

Query:

Please provide caption for Fig. 2.

Answer: Fig. 2 – **S**implified structural map of southwest Sicily offshore (adapted from **Argnani et al., 1987**; **Antonelli et al., 1988**; **Civile et al., 2018)** and onshore (modified after **Basilone, 2012)**. Focal mechanism in the foreland area from **Soumaya et al. (2015)**. Isobaths of the Pliocene-Quaternary from the **Structural Model of Italy (Bigi et al., 1989).** The bathymetric metadata and Digital Terrain Model data products have been derived from the EMODnet Bathymetry portal - http://www.emodnet-bathymetry.eu. Labels are as follow: ATF, Adventure Thrust Front; CGFS, Capo Granitola Fault System; SFS, Sciacca Fault System; GNF, Gela Nappe Front; MV, Mazara del Vallo; CG, Capo Granitola; CV, Castelvetrano; CSM, Capo San Marco; SA, Sciacca; GB, Graham Bank; TB, Terribile Bank; NB, Nerita Bank.

Query:

Please provide caption for Fig. 3.

Answer: Fig. 3 – Trace of analysed seismic profiles and location of wells. MV, Mazara del Vallo; CG, Capo Granitola; SE, Selinunte; CSM, Capo San Marco; CV, Castelvetrano; SA, Sciacca; GB, Graham Bank; TB, Terribile Bank; NB, Nerita Bank. The topo-batymethric base map combines Emodnet bathymetry (http://www.emodnet-bathymetry.eu) and SRTM 30 plus topography (Shuttle Radar Tomography Mission, http://topex.ucsd.edu/WWW_html/srtm30_plus.html).

Query:

Please provide caption for Fig. 4.

Answer: Fig. 4 - Stratigraphic correlation among selected wells in the Saccense offshore domain (partly adapted from Civile et al., 2018). Location of wells in Fig. 3.

Query:

Please provide caption for Fig. 5.

Answer: Fig. 5 - Seismostratigraphic scheme of the investigated area as derived combining a part of an ENI MCS profile offshore Capo Granitola (**Fig. 8b**) and lithofacies data from Oscar-W well. The chart includes sub-units and related horizons detected in SCS profiles. Correlation between seismic units and sub-units, stratigraphy and seismic velocities based from facies analysis, stratigraphic data onshore this area (adapted from **Basilone, 2012)**, and lithostratigraphy and sonic log data available from wells drilled through coeval deposits offshore southern Sicily (see **Pepe et al., 2010** for details). BLT, basal surface of the last transgression; TMS, Top of Marsala Synthem; BMS, Base of Marsala Synthem; M, top of evaporites deposited during the late Messinian salinity crisis or the erosional unconformity formed during the late Messinian sea-level fall; Y, Base of evaporites deposited during the late Messinian salinity crisis; C, contact between the top of pre-orogenic carbonates and the base of Middle-Upper Miocene synorogenic silty-clay deposits.

Query:

Please provide caption for Fig. 6.

Answer: Fig. 6 - Seismostratigraphic interpretation of SCS profiles in the shallow shelf and above structural highs. Limits of seismic units, sub-units and unconformities are evidenced by thick dotted lines. S1a, S1b and S1c, sub-units of unit S1 recognised on SCS profiles. S2 and S3, seismic units (see figure 5 for details). BLT, Base of the Last Transgression; TMS, Top of Marsala Synthem; BMS, Base of Marsala Synthem; TTR, Top of Trubi formation; M, top of evaporites deposited during the late Messinian salinity crisis or the erosional unconformity formed during the late Messinian sea-level fall.

Query:

Please provide caption for Fig. 7.

Answer: Fig. 7 – Structural map of the Capo Granitola and Sciacca Fault Systems derived from integration of MCS and SCS data. Faults partly adapted from **Civile et al., 2018**). Northern and southern segments of the CGFS and SFA are indicated. Morpho-bathymetric map from GeoMapApp database (http://www.geomapapp.org). CGFS: Capo Granitola Fault System; SFS: Sciacca Fault System; CGF1, CGF2, Capo Granitola Faults 1, 2; SF1, Sciacca Fault 1; CGA, Capo Granitola Anticline (CGA-N, Northern segment; CGA-S, Southern segment; CGA1, CGA2, anticlines 1 and 2 mapped in SCS profiles); SA, Sciacca Anticline (SA-N, Northern segment; SA-S, Southern segment (Nerita Bank); SA-2, Southern segment 2 (Terribile Bank); SA-N/a, SA-N/b, anticlines a and b of northern segment mapped in

SCS profiles);. Other labels as in Figure 3.

Query:

Please provide caption for Fig. 8.

Answer: Fig. 8 - Interpreted MCS profiles across the northern segment of the CGFS (see also **Fig. 7** for location on the structural map of the Capo Granitola and Sciacca Fault Systems): a) part of profile C-1007 from the Vi.DE.PI database; b) part of Eni profile C81-33. GS, growth strata; S1 – S5, seismic units (see figure 5 for details); B, horizon that mark the upper limit of the axial surface that dip toward the CGA; M, top of evaporites deposited during the late Messinian salinity crisis or the erosional unconformity formed during the late Messinian sea-level fall; Y, Base of evaporites deposited during the late Messinian salinity crisis; C, contact between the top of pre-orogenic carbonates and the base of Middle-Upper Miocene synorogenic silty-clay deposits. CGF1, CGF2, Capo Granitola Faults 1 and 2.

Query:

Please provide caption for Fig. 9.

Answer: Fig. 9 - Depth-converted SCS profiles showing the shallow expression of CGA1 and CGA2 anticlines on top of the CGA (see also **Fig. 7** for location on the structural map of the Capo Granitola and Sciacca Fault Systems**;** position relative to the CGA in **Fig. 8a**). S1a, S1b and S1c, sub-units of unit S1 recognised on SCS profiles. S2 and S3, seismic units (see figure 5 for details). BMS, Base of Marsala Synthem; TTR, Top of Trubi formation; M, top of evaporites deposited during the late Messinian salinity crisis or the erosional unconformity formed during the late Messinian sea-level fall. GS, growth strata; SBM, Sea-Bottom Multiple.

Query:

Please provide caption for Fig. 10.

Answer: Fig. 10 - Interpreted MCS profiles across the northern (a) and southern (b) segments of the SFS (see also **Fig. 7** for location on the structural map of the Capo Granitola and Sciacca Fault Systems). S1 – S5, seismic units (see figure 5 for details); B, horizon that mark the upper limit of the axial surface that dip toward the CGA; TTR, Top of Trubi formation; M, the erosional unconformity formed during the late Messinian sea-level fall; C, contact between the top of pre-orogenic carbonates and the base of Middle-Upper Miocene synorogenic silty-clay deposits. SA, Sciacca Anticline; SF1, SF8, Transpressive faults indicated in Fig. 7.

Query:

Please provide caption for Fig. 11.

Answer: Fig. 11 - Depth-converted SCS profiles showing the shallow expression of the northern Sciacca Anticline (see also **Fig. 7** for location on the structural map of the Capo Granitola and Sciacca Fault Systems**;** position relative to the deep fold in **Fig. 10a**). S1a and S1b, sub-units of unit S1 recognised on SCS profiles. BLT, Base of the Last Transgression; S, apparent slip; SBM, Sea-Bottom Multiple.

Query:

Please provide caption for Fig. 12.

Answer: Fig. 12 – Quantitative analysis of the CGFS and SFS: a) Fold amplitude vs. distance from the coast along the CGA (northern and southern segments), and along the CGA1 and CGA2; b) Fold amplitude vs. distance from the coast along the SA (northern and southern segments) and along folds SA-N/a and SA-N/b. The segment boundaries and the pre- and post-linkage amplitudes are indicated. The name of MCS lines is reported on top of each diagram.

Query:

Please provide caption for Fig. 13.

Answer: Fig. 13 - Fold amplitude of horizon BMS for a) CGA1; b) CGA2, and of horizon TMS for c) SA vs. distance from the coast, based on SCS reflection profiles analyses. Same horizontal scale, vertical scale variable.

Query:

Please provide caption for Fig. 14.

Answer: Fig. 14 – Growth history of the Capo Granitola and Sciacca anticlines showing incremental growth rates (see text). Maximum amplitudes for each horizon listed in Tab. 3. Horizon labels as in Fig. 5.

Query:

Your article is registered as a regular item and is being processed for inclusion in a regular issue of the journal. If this is NOT correct and your article belongs to a Special Issue/Collection please contact d.perumal@elsevier.com immediately prior to returning your corrections.

Answer: Yes

Query:

Please confirm that given names and surnames have been identified correctly and are presented in the desired order, and please carefully verify the spelling of all authors' names.

Answer: Yes

Query:

The author names have been tagged as given names and surnames (surnames are highlighted in teal color). Please confirm if they have been identified correctly.

Answer: Yes

Query:

Please check whether the designated corresponding author is correct.

Answer: correct

Query:

Highlights should consist of only 125 characters per bullet point, including spaces. However, the Highlights provided for this item exceed the maximum requirement. Kindly provide replacement Highlights that conform to the requirement for us to proceed. For more information, please see the Guide for Authors.

Answer: new highlights in attached file
Attachments: Highlights.docx

Query:

Please check the hierarchy of the section headings and confirm if correct.

Answer: Yes

Query:

Uncited references: This section comprises references that occur in the reference list but not in the body of the text. Please position each reference in the text or, alternatively, delete it. Thank you.

Answer: The references are not in the text but in the captions provided in previous queries; and so they should be included in the reference list

Query:

Correctly acknowledging the primary funders and grant IDs of your research is important to ensure compliance with funder policies. We could not find any acknowledgement of funding sources in your text. Is this correct?

Answer: Yes